Applied Catalysis B: Environmental 224 (2018) 810–824

Contents lists available at ScienceDirect

Applied Catalysis B: Environmental

journal homepage: www.elsevier.com/locate/apcatb

Research Paper

Removal of antibiotics, antibiotic-resistant bacteria and their associated genes by graphene-based TiO_2 composite photocatalysts under solar radiation in urban wastewaters

Popi Karaolia[a,b], Irene Michael-Kordatou[a], Evroula Hapeshi[a], Catherine Drosou[c], Yannis Bertakis[c], Dimitris Christofilos[d], Gerasimos S. Armatas[e], Labrini Sygellou[f], Thomas Schwartz[g], Nikolaos P. Xekoukoulotakis[c,**], Despo Fatta-Kassinos[a,b,*]

[a] Nireas-International Water Research Center, University of Cyprus, P.O. Box 20537, 1678, Nicosia, Cyprus
[b] Department of Civil and Environmental Engineering, School of Engineering, University of Cyprus, P.O. Box 20537, 1678, Nicosia, Cyprus
[c] Department of Environmental Engineering, Technical University of Crete, GR-73100, Chania, Greece
[d] Chemical Engineering Department, Aristotle University of Thessaloniki, GR 54124, Thessaloniki, Greece
[e] Department of Materials Science and Technology, University of Crete, GR 71003, Heraklion, Greece
[f] Foundation of Research and Technology Hellas, Institute of Chemical Engineering and High Temperature Chemical Processes (FORTH/ICE-HT), P.O. Box 1414, GR 26504, Rion, Patras, Greece
[g] Institute of Functional Interfaces, Karlsruhe Institute of Technology, Hermann-von-Helmholtz-Platz 1, Eggenstein-Leopoldshafen, 76344, Germany

ARTICLE INFO

Keywords:
Graphene
TiO_2 photocatalysis
Antibiotics
Antibiotic-resistant bacteria
Antibiotic resistance genes

ABSTRACT

The present work investigated: (i) the removal of the antibiotics sulfamethoxazole (SMX), erythromycin (ERY) and clarithromycin (CLA); (ii) the inactivation of the total and antibiotic-resistant *E. coli* along with their re-growth potential after treatment; (iii) the removal of the total genomic DNA content; and (iv) the removal of selected antibiotic resistance genes (ARGs), namely *sul*1, *amp*C, *erm*B, *mec*A, as well as species-specific sequences, namely *ecf*X for *Pseudomonas aeruginosa* and enterococci-specific 23S rRNA, by graphene-based TiO_2 composite photocatalysts under solar radiation, in real urban wastewaters. TiO_2-reduced graphene oxide (TiO_2-rGO) composite photocatalysts were synthesized by two *ex-situ* synthesis methods, namely hydrothermal (HD) treatment and photocatalytic (PH) treatment, starting from graphene oxide and Aeroxide P25 TiO_2, and were characterized with various techniques, such as XRD, FT-IR, Raman, XPS, SEM and surface area (BET) analyses. The potential of the synthesized TiO_2-rGO composites for the removal of the abovementioned antibiotic-related microcontaminants was compared to the efficiency shown by pristine Aeroxide P25 TiO_2 under simulated solar radiation, in real urban wastewater effluents treated by a membrane bioreactor. The results showed that TiO_2-rGO-PH was more efficient in the photocatalytic degradation of ERY (84 ± 2%) and CLA (86 ± 5%), while degradation of SMX (87 ± 4%) was found to be slightly higher with Aeroxide P25 TiO_2. It was also demonstrated that more than 180 min of treatment were satisfactory for the complete inactivation and complete absence of post-treatment regrowth of *E. coli* bacteria (< LOD) even 24 h after the end of the treatment, for all examined photocatalytic materials. The least amount of regrowth at all experimental times was observed in the presence of TiO_2-rGO-HD. Moreover, the synthesized graphene-based photocatalysts successfully removed *amp*C and significantly reduced *ecf*X abundance of *Pseudomonas aeruginosa*, but *sul*1, *erm*B and 23S rRNA for enterococci sequences were found to be persistent throughout treatment with all catalyst types. Finally, the total DNA concentration remained stable throughout the photocatalytic treatment (4.2–4.8 ng μL^{-1}), indicating the high total genomic DNA stability in treated wastewater and its resistance to photocatalytic treatment.

1. Introduction

As the potential function of treated wastewater reuse as an alternative source of water supply is now well acknowledged and embedded within international, European, and national strategies, there have been concerted efforts which specifically target a substantial

* Corresponding author at: Nireas-International Water Research Center, University of Cyprus, P.O. Box 20537, 1678, Nicosia, Cyprus.
** Corresponding author at: Department of Environmental Engineering, Technical University of Crete, GR-73100, Chania, Greece.
E-mail addresses: nikos.xekoukoulotaki@enveng.tuc.gr (N.P. Xekoukoulotakis), dfatta@ucy.ac.cy (D. Fatta-Kassinos).

https://doi.org/10.1016/j.apcatb.2017.11.020
Received 28 July 2017; Received in revised form 7 November 2017; Accepted 9 November 2017
Available online 10 November 2017
0926-3373/

increase in recycling and safe wastewater reuse globally by 2030 [1]. Consequently, wastewater treatment plants (WWTPs) offer a highly promising source of recycled water to deal with issues of water scarcity and water quality deterioration in problematic areas. However, the observation of the presence of xenobiotic microcontaminants of emerging concern in treated wastewater effluents makes the task of wastewater reuse a challenging one.

An increase in the abundance of antibiotics due to their overuse, misuse, and incomplete removal by the conventional processes applied in WWTPs, accompanied by an increase in the prevalence of antibiotic-resistant bacteria (ARB) and their associated antibiotic resistance encoding genes (ARGs) has been observed in the last decades in treated wastewater effluents [2,3]. Their presence has been well established in these waters [2,3], suggesting the dominance of these aquatic matrices as potential pathways of human exposure to wildlife strains of ARB, and their associated ARGs [4]. Furthermore, treated wastewater used for irrigation has also been shown to be implicated in the transmission of water-borne pathogenic bacteria, which has led to the implementation of rigorous controls on the discharged effluent microbiological quality intended for irrigation, in various countries [5,6].

ARGs, which may be encoded in bacterial chromosomes or in extrachromosomal plasmids, can elicit biochemical defence mechanisms that allow the survival of bacteria in the presence of the corresponding antibiotic compounds such as in the case of treated wastewater, thus making them increasingly resilient in conditions of environmental stress, *i.e.* during wastewater treatment. Also, plasmid-elicited resistance genes bear the potential of attainment by suitable, previously antibiotic-susceptible bacteria through the horizontal gene transfer (HGT) mechanisms of conjugation, transformation, and transduction [7]. Especially conjugative transfer mechanisms are highly common in natural environments where there is a high density of metabolically active bacterial cells which have a close proximity to each other, making the exchange of genetic material such as ARGs, possible [8,9].

WWTPs, whose operation is typically based on biological treatment, such as the conventional activated sludge process, have been indicated as imperative hubs of ARB development and ARGs dissemination [2,10], as there may be an absence of disinfection process or the existing disinfection process, such as chlorination, ozonation and UV radiation, may be inadequate for the successful inactivation of ARB and removal of genomic DNA and ARGs [11,12]. Consequently, novel disinfection and decontamination processes, such as advanced oxidation processes (AOPs), must be investigated to establish their efficiency for the removal of organic microcontaminants in urban treated effluents. The potential of AOPs for the disinfection of urban wastewater effluents has been previously investigated [13], but the potential of these techniques for the removal of other microbiological components such as ARGs, has not been thoroughly studied. As these processes involve the *in-situ* generation of powerful oxidative transient species, such as free hydroxyl radicals (HO·), they have a strong oxidation potential for a wide range of organic microcontaminants, such as antibiotic compounds, as well as a potential for bacterial cell and DNA damage [14].

Heterogeneous TiO_2 photocatalysis is an AOP with a wide variety of technological applications, including its use for the inactivation of pathogenic microorganisms [15–18]. It has emerged as a viable option for disinfection, as it possesses the advantage of utilization of natural or artificial solar radiation for its operation, reducing the cost of the process, while making this operation an environmentally sustainable one [15–18]. Due to its associated advantages, various modifications of the TiO_2 photocatalytic process have been suggested, including coupling of TiO_2 with graphene-based materials [15,19–24]. Graphene is a two-dimensional nanocarbon material, composed of single-, bi- or few- ($\leq$10) layers of fused sp^2 hybridized carbon atoms, forming six-membered rings which are arranged into a honeycomb-like lattice [25–27]. The properties that make it an appealing material for disinfection and decontamination purposes include: (i) high specific surface area, thus increasing adsorption of microcontaminants onto TiO_2-graphene composites; (ii) high transparency due to its one-atom thickness; (iii) extended light absorption range towards the visible region of the electromagnetic spectrum; and (iv) outstanding electron mobility due to its delocalized conjugated π structures. The result of these features is the facilitation of charge transportation and electron/hole separation in TiO_2, contributing to the enhancement of the photocatalytic activity of synthesized photocatalytic materials, including TiO_2, as demonstrated in various recent studies [15,19–24]. As an outcome, it is suggested that highly conductive rGO could be considered as the ideal material for the improvement of semiconductor photocatalytic materials, as it not only has the potential to serve as an excellent electron acceptor for the restriction of photo-generated electron-hole pair recombination, but also bears various inherent photocatalytic advantages such as its unique two-dimensional carbon structure (sp^2-hybridization), its excellent conductivity and a large surface area [15,19–24].

Although numerous papers have been published on the photocatalytic degradation of several organic pollutants in the aqueous phase employing various graphene-based composite TiO_2 photocatalysts [15,19–24], there is a rather limited number of studies dealing with the photocatalytic disinfection of different microorganisms in the presence of graphene-based TiO_2 composite materials [14–18,22,28–43]. Indeed, various studies have demonstrated the improvement of disinfection of *E. coli* under natural or simulated solar radiation by graphene-based TiO_2 composite photocatalysts in different forms, including platelets, nanorod composites, and loose fine powder. Increased antibacterial action was reported by the composites, compared to the efficiency of TiO_2 alone in the conducted studies. The observed increased inactivation effect compared to the effect of TiO_2 alone was attributed to the two-dimensional sheet support, to the large surface area and to the increased adsorption capacity [14–18,22,28–43]. For example, Fernández-Ibáñez et al. [14] synthesized TiO_2–rGO composites which were compared to Aeroxide P25 TiO_2 in suspension reactors, for the disinfection of water from *E. coli* and *Fusarium solani* spores, under real solar radiation. An increase in the inactivation of *E. coli* was observed using the TiO_2–rGO composites compared to TiO_2 alone, while when the major part of the UVA radiation was cut-off ($\lambda > 380$ nm) with a methacrylate screen, there was a significant rise in the *E. coli* inactivation time required with TiO_2, but no change in the inactivation rate by TiO_2–rGO.

Despite the extended investigation of the removal efficiency of synthesized TiO_2-rGO of microcontaminants, including antibiotics and bacteria [15–19,29–44], no studies have gone the extra mile to investigate the disinfection potential of the synthesized composites regarding a mixture of various antibiotic-related microcontaminants, including antibiotics, important indicator bacterial species, ARB&ARGs in a real urban wastewater, simulating a real-case scenario, as well as their potential for elimination of bacterial regrowth. Based on the above, the aim of the present study was to synthesize TiO_2-rGO composite materials and to investigate for the first time their photocatalytic efficiency in real wastewater, for the abatement of a diverse array of antibiotic-related chemical and microbiological microcontaminants, more specifically: (i) a mixture of various antibiotics including a selection which has been included in the EU Watch list of substances for Union-wide monitoring, as they may pose a significant risk to aquatic environments [44], namely clarithromycin (CLA), erythromycin (ERY), and sulfamethoxazole (SMX); (ii) the inactivation of total bacteria, ARB (*Escherichia coli*) and their regrowth potential after treatment; (iii) the removal of total genomic DNA content which may contain ARGs; and (iv) ARGs (*amp*C, *sul*1, *mec*A, *erm*B) and species specific marker sequences (*Enterococcus* spp. and *Pseudomonas aeruginosa*) using molecular qPCR analyses. Another novelty of this study is the investigation of the above parameters in a real wastewater effluent, which has previously been treated with a Membrane BioReactor (MBR) giving a highly clarified final effluent (final effluent inherent *E. coli* concentrations: 2 CFU 100 mL^{-1}, < LOD), thus making it an ideal matrix for the kinetic investigation of the inactivation of spiked indigenous high

bacterial concentrations (approximate initial spiked concentration of 1×10^6 CFU mL^{-1}) during photocatalytic disinfection experiments. To the authors' knowledge, this is the first study to compare the disinfection, inactivation, and decontamination of an array of antibiotic-related microcontaminants by graphene-based materials in real wastewater effluents, under simulated solar radiation.

2. Experimental

2.1. Materials and reagents

Clarithromycin (CLA, ≥98%, Chemical Abstract Service (CAS) Number 81103-11-9, molecular formula $C_{38}H_{69}NO_{13}$, molecular weight 747.95 g mol^{-1}), erythromycin (ERY, ≥98%, CAS Number 114-07-8, molecular formula $C_{37}H_{67}NO_{13}$, molecular weight 733.93 g mol^{-1}) and sulfamethoxazole (SMX, CAS Number 723-46-6, molecular formula $C_{10}H_{11}N_3O_3S$, molecular weight 253.28 g mol^{-1}) were purchased from Fluka Analytical and were used as received. Graphite was obtained from Alfa Aesar (graphite powder, synthetic, ~325 mesh, 99.9995%) and was used as received. Aeroxide P25 TiO_2 was kindly supplied from Evonik Industries. Ethanol (LC–MS grade) was obtained from Sigma-Aldrich. The solvents used for the chromatographic analysis were acetonitrile (Sigma-Aldrich) and methanol (Fluka). Ultrapure water (resistivity 18.2 MΩ cm^{-1} at 25 °C), employed for solution preparation and as eluent, was prepared on a Merck Millipore water purification system.

2.2. Synthesis of TiO_2-rGO composite photocatalysts

Graphite oxide was synthesized by a modified Hummers and Offeman's oxidation method [45] as described in detail in the Supplementary data (text S1), while exfoliation of graphite oxide to aqueous suspensions of graphene oxide (hereafter denoted as GO) was performed by ultrasonic irradiation, as also described in detail in the Supplementary data (text S1).

The preparation of TiO_2-rGO composite photocatalysts has been performed by two *ex-situ* methods, namely: (i) by hydrothermal treatment, *i.e.* by heating a suspension of TiO_2 and exfoliated GO in a mixture of ultrapure water and ethanol at elevated temperature (above 100 °C) and pressure (above 1 bar) [46]; and (ii) by photocatalytic treatment, *i.e.* by irradiating a suspension of TiO_2 and exfoliated GO in ethanol under UVA radiation and anoxic conditions [46,47]. During hydrothermal and photocatalytic treatment, exfoliated GO sheets were partially reduced, thus forming rGO, and at the same time TiO_2 was incorporated in the framework of rGO, thus forming TiO_2-rGO composites. More details are given in the Supplementary data (text S2).

2.3. Characterization of photocatalytic materials

X-ray diffraction (XRD) patterns were collected on a PANanalytical X'pert Pro MPD X-ray diffractometer using Cu Kα radiation (λ = 0.15406 nm, 45 kV, and 40 mA) in Bragg–Brentano geometry. Fourier transform infrared spectroscopy spectra (FT-IR) of the solid samples were recorded on a Perkin–Elmer Spectrum 1000 spectrometer between 4000 and 400 cm^{-1} in KBr pellets. Raman measurements were conducted with a Horiba Lab RAM HR spectrometer equipped with a Peltier-cooled charge coupled device. Excitation was provided by the 514.5 nm line of an Ar^+ laser with a laser power of ~15 μW focused on the sample by a standard 100 × objective in a spot with a diameter of ~1 μm. The signal was collected from an area of 10 × 10 μm^2, taking advantage of a DuoScan™ scanner, which allows fast scanning of the laser beam on the examined sample. All spectra were normalized to one accumulation time and as to the laser power, to have comparable Raman intensities. Thus, the average power on the sample is very low without reduction in the Raman signal, and the Raman spectrum is more representative of the sample.

Nitrogen adsorption-desorption isotherms were measured at −196 °C on a Quantachrome NOVA 3200e sorption analyzer. Prior to the measurement, all samples were outgassed at 80 °C under vacuum ($< 10^{-5}$ Torr) for 12 h. The specific surface areas were calculated using the Brunauer-Emmett-Teller (BET) method on the adsorption data in the relative pressure range of 0.05–0.26. The total pore volumes were estimated from the adsorbed amount at the relative pressure of $P/P_o = 0.98$. Scanning electron microscopy (SEM) images were taken with a JEOL JSM-6390LV electron microscope operated at 20 kV. Samples were gently placed on carbon tape, forming flat surfaces, and brought into the instrument chamber for analysis.

The X-ray photoelectron spectroscopy (XPS) measurements were carried out in an ultra-high vacuum system, which consists of a fast entry specimen assembly, a sample preparation, and an analysis chamber. The base pressure in both chambers was 1×10^{-9} mbar. Unmonochromatized AlKα line at 1486.6 eV and an analyzer pass energy of 97 eV, giving a full width at half maximum of 1.7 eV for the Au $4f_{7/2}$ peak, were used in all XPS measurements. The XPS core level spectra were analyzed using a fitting routine, which can decompose each spectrum into individual mixed Gaussian-Lorentzian peaks after a Shirley background subtraction. Regarding the measurement errors, for the XPS core level peaks it was estimated that for a good signal to noise ratio, errors in peak positions were about ± 0.05 eV. The calibration of the analyzer's kinetic energy scale was done according to ASTM-E 902-88. The samples were in powder form and pressed in stainless steel pellets.

2.4. Experimental setup and procedure

To examine the photocatalytic treatment efficiency for the decontamination of antibiotics and inactivation of total bacteria, of ARB and removal of ARGs, a real MBR-treated wastewater effluent was chosen due to its very low inherent antibiotic concentrations (inherent concentrations of the examined antibiotics: 5.5–7.2 ng L^{-1}), very low total bacterial concentrations (final effluent inherent *E. coli* concentrations: 2 CFU 100 mL^{-1}, < LOD) and high-quality physicochemical characteristics. These characteristics make the MBR-treated effluent an ideal matrix for the kinetic investigation of the removal of the spiked antibiotics (C_0 = 100 μg L^{-1}) and for the inactivation of indigenous wastewater bacterial concentrations ($C_0 = 1 \times 10^6$ CFU mL^{-1} of *E. coli*) during photocatalytic disinfection experiments.

At the time of the experimental procedure, the MBR pilot unit, which is designed to treat 10 m^3 d^{-1} of sewage, was situated at the premises of the University of Cyprus. There are 25 flat-sheet membrane cartridges (Kubota, Japan) with a total functional surface area of 100 m^2 and the membrane nominal pore diameter is 0.4 μm. The estimated hydraulic retention time (HRT) was 30 days, while the solids retention time (SRT) was 9 h. More information on the physicochemical characteristics of the water matrix are given in Supplementary data (Text S3).

For the photocatalytic experiments, a laboratory-scale solar simulator Newport type 91193 (1 kW Xenon lamp) was used. The irradiation intensity of the simulator was determined using 2-nitrobenzaldehyde (purchased from Sigma-Aldrich) as a chemical actinometer [48] and it was found to be 63 W m^{-2}. Experiments were conducted in a double-walled Pyrex glass batch reactor (inner diameter 8 cm, height 9.5 cm). The experiments were conducted at the inherent solution pH, which was slightly acidic (range of pH 5.2–6.2), under air-equilibrated conditions. Throughout the experimental procedure, the temperature was controlled (25 ± 1 °C) with the use of a thermostatic bath.

The stock solutions of the examined antibiotics used for the experiments were prepared using the appropriate solvent followed by subsequent dilution in water. In a typical photocatalytic run, an appropriate volume from the stock solution was added to the reactor in order to reach 100 μg L^{-1} of the substrate in a 300-mL volume of the MBR effluent. After careful bibliographic review, this concentration of

antibiotics has been chosen as it is slightly higher than environmentally-relevant concentrations of the examined antibiotics in the aquatic environment, in order to provide the process efficiency within a measurable time scale and accurately determine the efficiency of degradation of the antibiotics examined in this work [49].

Following, the desired catalyst concentration of 100 mg L^{-1} was completely suspended in slurry in the spiked effluent using sonication (10 min) followed by magnetic stirring at 500 rpm (30 min) for antibiotics removal and 60 min for total bacteria and ARB inactivation and genomic DNA, species-specific genes and ARGs removal in the dark, to ensure complete equilibration of adsorption/desorption of the three antibiotics, onto the catalyst surface, or to observe the effect of the catalyst particles on the bacteria in suspension. The catalyst concentration of 100 mg L^{-1} was chosen based on a bibliographic review, as it produces a lower operational cost of catalyst use and it gives the advantage of easy catalyst regeneration and removal from the treated suspension. After that period, the solar lamp was turned on for a total photocatalytic treatment time of 60 min for antibiotics, and for 180 min for total bacteria and ARB inactivation and genomic DNA, species-specific genes and ARGs removal examination. The exact procedure for the preparation of the bacterial inoculum is given in the Supplementary data (Text S4). The difference in examined microcontaminant concentration among the times between the first sample in the dark and the next sample at the point when the lamp was turned on and the photocatalytic reaction began (T_0 was considered as the zero photo-reaction time), established the degree of: i) adsorption of the spiked antibiotic compounds, ii) inactivation of the spiked total and ARB, iii) reduction of total genomic DNA or of ARGs due to the presence of the solid catalyst particles, in dark conditions. For the determination of antibiotic concentrations, aliquots (2 mL) were drawn from the photo-irradiated reactor at pre-defined time intervals using 5 mL syringes and were then filtered through 0.22 μm PES filters (Agilent) and injected into 2 mL glass vials for chromatographic analysis.

All experiments were performed in triplicates. Average values are shown as results and the uncertainty that is stated as the standard deviation between measurements never exceeded 15%. Initially, hydrolysis and photolysis experiments were conducted to establish any hydrolysis effect and the impact of sole simulated solar light on the examined microcontaminants.

The determination of the Minimum Inhibitory Concentration (MIC) for the ARB selection was conducted according to the CLSI standard methods for dilution antimicrobial susceptibility tests for bacteria that grow aerobically [50]. Detailed information on the MIC determination can be found in Supplementary data (Text S5).

2.5. Analytical methods

2.5.1. Analytical methods for the determination of physicochemical characteristics

Temperature and pH were measured using a pH meter (EZDO, PL-600). Conductivity was measured using an electronic conductivity meter (EZDO, CTS-506). Dissolved oxygen was measured using an oxygen meter (EZDO, PDO-408). The Chemical oxygen demand (COD) of samples was determined using the Merck Spectroquant® cell tests (Merck). The DOC was measured using a TOC analyzer (Aurora 1030).

2.5.2. Analytical methods for the determination of total and antibiotic-resistant E. coli

The limit of detection (LOD) of the method used for the viability testing (membrane filtration method) of *E. coli* was 2 CFU 100 mL^{-1}. Detailed information on the methods used for the determination of total and antibiotic-resistant *E. coli* can be found in Supplementary data (Text S6).

In addition to the hydrolytic and photolytic effect investigation on the viability of the selected type of bacteria, a control sample was taken prior to light exposure which was kept in the dark, and plated out twice, once at the time of sampling and the at the end of the experiment. This control ensured the cell viability without any of the treatments.

As various bacteria were shown to enter a viable but not cultivable (VBNC) state during/after wastewater treatment, they may still be alive but not appearing on cultivation media, while still having the potential of re-activation and regrowth during storage and distribution of treated effluents [51]. Consequently, the photocatalytic experiment duration that was able to completely and permanently halt regrowth of bacteria was investigated. The regrowth of *E. coli* at all experimental times was examined, in order to check whether the reduction in bacteria signified their permanent inactivation, or their injuring and temporary inactivation, which could lead to their regrowth after allowing a specific amount of time for repair/reactivation.

As a result, for the examination of the regrowth of *E. coli* after photocatalytic treatment and subsequent storage in a dark place, 1 mL samples were taken at each experimental time in a sterile container in the dark, and incubated at 44 °C for 24 h. This incubation temperature of the treated samples was selected for a dual purpose: it is the optimum temperature of *E. coli* growth [52] and it represents the real-life scenario of treated wastewater storage in Mediterranean countries, where external tank storage temperatures may be very high, compared to Central and Northern countries. The ratio of the counted colonies (C_r) (CFU mL^{-1}) during the regrowth experiment to the colonies counted after photocatalytic treatment (C_t) was then calculated, as C_r/C_t. The ratios calculated that exceeded 1 at any experimental time, were considered as regrowth of damaged/inactivated bacteria that were previously unable to grow on the selective medium. So, bacterial numbers during the regrowth test exceeding the bacterial numbers encountered during the photocatalytic treatment, are considered as repaired/reactivated bacteria that were previously damaged/inactive and were unable to grow on solid media (non-cultivable) due to the photocatalytic treatment.

2.5.3. Analytical methods for the determination of total genomic DNA, of species-specific genes and of ARGs

For the determination of the species-specific genes and of ARGs, a separate batch of experiments without any spiked ARB or antibiotics was conducted in order to determine the impact of the photocatalytic process using the examined types of photocatalytic matetrials, on the inherent DNA concentration and on the prevalence of selected genes. The treated samples were stored at 4 °C in the dark, until analysis, within 24 h of sampling. Due to the low concentration of total genomic DNA in wastewater after MBR treatment, in order to obtain the desired DNA concentration following DNA extraction, 500 mL of the treated solution were used for each DNA extraction.

Primarily, the samples were filtered through 45 mm polycarbonate filter membranes with a 0.22 μm pore size (Millipore). Following, the DNA extraction took place from the collected samples, using the PowerWater® DNA isolation Kit (MoBio) following the manufacturer's protocol. The quantity and purity of the DNA extracts was measured using the NanoDrop ND-1000 instrument (PeqLab Biotechnology, Erlangen, Germany).

The DNA content can give an initial indication of the microbial density inside a target matrix, where the transfer and exchange of environmentally- and clinically-relevant ARGs targets among non-pathogenic bacterial fractions can take place *via* HGT, contributing to the risk of the spread of antibiotic resistance (AR) in the aquatic environment [53,54]. Therefore, the evaluation of the DNA concentration and the calculation of $\log_{10}$ cell equivalent values (CE) make a reliable means of assessment of the overall relative genetic abundance and of the genetic flow in bacterial communities of water environments.

For the quantitative PCR analyses (qPCR), the specific primers used to quantify ARGs and opportunistic bacteria in 100 ng of total DNA are given in Table 1. A real time quantitative PCR assessment was carried out using the Bio-Rad CFX 96 Touch™ Real-Time PCR Detection System. The exact analytical procedure followed, is provided in Supplementary

Table 1
The specific primers of qPCR analysis.

Sequence name		Target	Species	Sequence	Reference
ampC-FP	Ampicillin resistance	Beta-lactamase	*Enterobacter* spp.	GGGAATGCTGGATGCACAA	[84]
ampC-RP				CATGACCCAGTTCGCCATATC	
qSUL1_653F	Sulfonamide resistance	Dihydropteroate synthase		CCGTTGGCCTTCCTGTAAAG	[85]
qSUL1_719r				TTGCCGATCGCGTGAAGT	
ECST784F	Enterococcus specific	23S rRNA	*Enterococcus* spp.	AGAAATTCCAAACGAACTTG	[84]
ENC854R				CAGTGCTCTACCTCCATCATT	
mecA1FP	Methicillin resistance	Chromosomal penicillin-binding protein 2a	*Staphylococcus* spp.	CGCAACGTTCAATTTAATTTTGTTAA	[84]
mecA1RP				TGGTCTTTCTGCATTCCTGGA	
ermB-F	Erythromycin resistance	Erythromycin-ribosome-methylase		TGAATCGAGACTTGAGTGTGCAA	[54]
ermB-R				GGATTCTACAAGCGTACCTT	
EcfXRT-F	Pseudomonas specific	RNA Polymerase Sigma-70 factor	*Pseudomonas aeruginosa*	AGCGTTCGGTCCTGCACAAGT	[86]
ecfXRT-R				TCCACCATGCTCAGGGAGAT	

data (text S7).

2.5.4. Analytical methods for determination of antibiotics

The sample extracts were injected directly into the UPLC–MS/MS system. For the determination of inherent antibiotic concentrations inside the MBR-treated effluent, solid phase extraction (SPE) of the samples took place before chromatographic analysis. The SPE procedure was carried out using OASIS HLB cartridges (3 cc, 60 mg) from Waters Corporation (Milford MA, USA). The method of SPE was described previously [55]. Target antibiotics in treated samples were extracted off-line at inherent pH. Prior to the SPE, the samples (100 mL) were filtered through a PVDF membrane filter (0.45 μm, Merck). The cartridges were conditioned with 5 mL methanol and 5 mL ultrapure water. Next, percolation of samples through the cartridges took place by gravity followed by washing with 5 mL water before drying under vacuum for 20 min. Finally, elution took place with 8 mL methanol followed by evaporation under a gentle nitrogen stream to dryness, at 40 °C. The dried samples were finally reconstituted in 1 mL of 25% aqueous solution of methanol.

The presence of antibiotics was monitored on an ACQUITY TQD UPLC–MS/MS system (Waters Corporation) equipped with a triple quadrupole mass spectrometer (TQD, serial number QBA012), operated in positive electrospray (ESI) mode. The most abundant product transition ions used are given in Table 2. The exact analytical protocol is provided in the Supplementary data (text S8).

3. Results and discussion

3.1. Synthesis of the TiO_2-rGO composite photocatalysts

As it is well-known form the literature, there are plenty of methods for synthesizing graphene-based composite materials, which can conceptually be divided into two general categories, *i.e.*, *in-situ* and *ex-situ* methods [21]. In the former general synthesis methods (*i.e.*, *in-situ*) an appropriate soluble precursor of the photocatalyst is employed, as well as a precursor of graphene (such as GO, amongst others), which are mixed in an appropriate solvent, followed by thermal, chemical, photochemical, or ultrasonic treatment. Moreover, in the *ex-situ* process, the photocatalyst itself, rather than its precursor, is mixed with the graphene precursor in an appropriate solvent, followed by thermal, chemical, photochemical, or ultrasonic treatment, thus resulting in the formation of the graphene-based composite photocatalyst. The main characteristic of the *in-situ* methods is that they usually lead to good interfacial contact between the photocatalyst and the graphene network, while they often suffer from low crystallinity of the photocatalyst. On the other hand, the main advantage of the *ex-situ* methods is that they employ pre-synthesized or commercially available photocatalyst, such as Aeroxide P25 TiO_2, with well-defined particle characteristics (such as crystallite size, shape, and morphology), which usually remain almost the same during their incorporation in the graphene-based composite photocatalysts [21].

Table 2
UPLC–MS/MS parameters established for the MRM acquisition mode.

Compound	Precursor ion (m/z) $[M+H]^+$	Cone voltage (eV)	Collision energy (eV)	Product ion (m/z)[a]
Clarithromycin	747	40	30	590
	747	40	20	158
Sulfamethoxazole	254	20	16	156
	254	21	25	92
Erythromycin	734.7	35	20	576.4
	734.7	35	30	158.1
	734.7	35	15	116.1

[a] Top: product ion used for quantification; below: the product ions used for confirmation.

Based on the above, for the synthesis of the TiO_2-rGO composite photocatalysts, two *ex-situ* synthetic procedures were employed, starting from Aeroxide P25 TiO_2 and exfoliated GO, namely hydrothermal and photocatalytic coupling [46,47], as described in detail in the experimental section and in the Supplementary data. Briefly, in the first preparation method, a suspension of Aeroxide P25 TiO_2 and exfoliated GO in a mixture of ultrapure water and ethanol in a 2:1 volume ratio, was transferred into a Teflon-lined high-pressure reactor and heated at 180 °C for 6 h. During this hydrothermal treatment, exfoliated GO was reduced to rGO, and at the same time, TiO_2 was anchored on the framework of rGO, thus resulting in the formation of the TiO_2-rGO-HD composite photocatalyst [46]. On the other hand, in the photocatalytic synthetic procedure, a suspension of Aeroxide P25 TiO_2 and exfoliated GO in ethanol was irradiated under UVA radiation in anoxic conditions [47]. Under these experimental conditions, electrons generated by UVA irradiation of TiO_2 were injected into GO, thus reducing the oxygen-containing functional groups and thereby partially restoring the conducting graphene network, while TiO_2 was simultaneously incorporated in the framework of rGO, thus resulting in the formation of the TiO_2-rGO-PH composite photocatalyst. Moreover, the photogenerated holes from TiO_2 were scavenged by ethanol to form ethoxy radicals, which were further oxidized to CO_2 and water [47].

3.2. Materials characterization

XRD patterns of graphite and graphite oxide are shown in Fig. 1a. The diffractogram of graphite shows the sharp 002 diffraction peak at $2\theta = 26.5^\circ$, which is characteristic of the highly-organized crystal structure of graphite. On the other hand, the XRD pattern of graphite oxide shows a broad 001 diffraction peak at about $2\theta = 11.9^\circ$, which demonstrates the typical loose-layer-like structure of graphite oxide. The interlayer spacing was calculated using Bragg's diffraction law at 0.34 nm and 0.74 nm for graphite and graphite oxide, respectively. The interlayer spacing of graphite oxide is higher than the corresponding

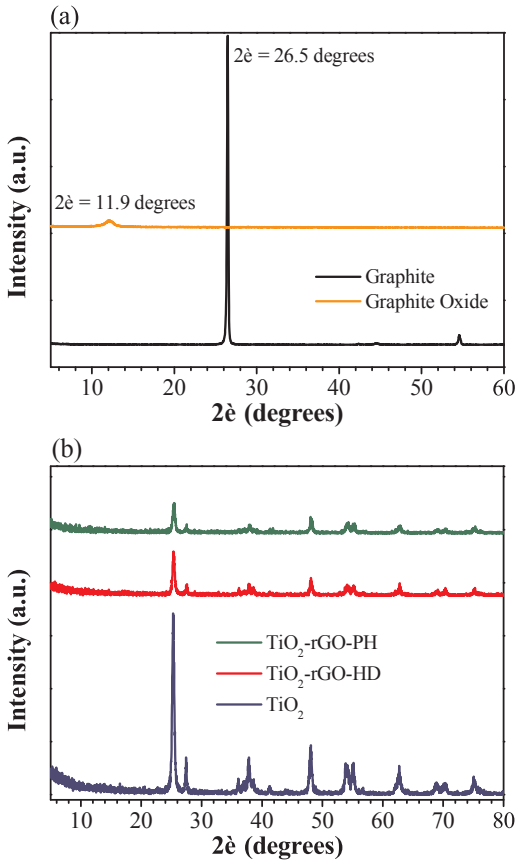

Fig. 1. XRD patterns of: (a) graphite and graphite oxide; and (b) TiO_2, TiO_2-rGO-HD and TiO_2-rGO-PH.

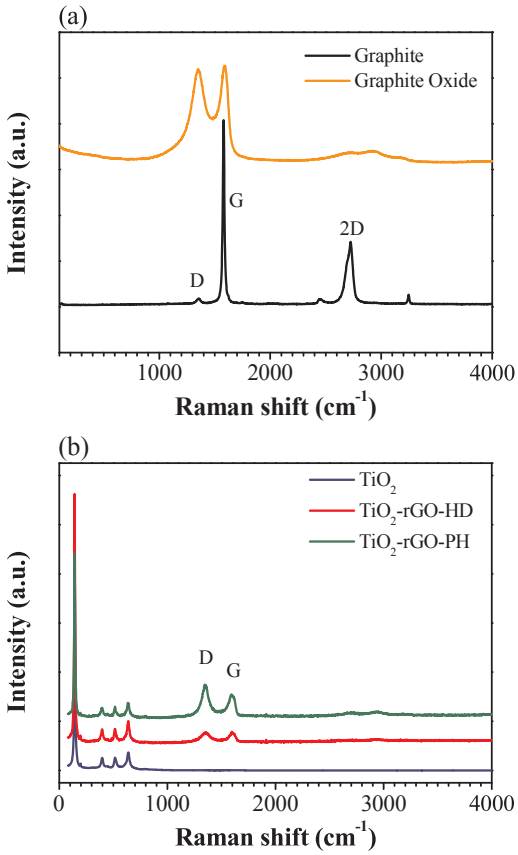

Fig. 2. Raman spectra of: (a) graphite and graphite oxide; and (b) TiO_2, TiO_2-rGO-HD and TiO_2-rGO-PH.

value in graphite because of the presence of oxygen-contained functional groups in the oxidized graphene layers of graphite oxide. Fig. 1b shows the diffractograms of TiO_2, TiO_2-rGO-HD, and TiO_2-rGO-PH. As can be seen in Fig. 1b, the diffractogram of Aeroxide P25 TiO_2 has all the characteristic peaks corresponding to the mixed crystallite phases of anatase and rutile TiO_2 [56]. Moreover, the diffractograms of the TiO_2-rGO composite photocatalysts do not show any significant differences compared to the diffractogram of TiO_2, which indicates that the coupling of TiO_2 with rGO does not cause any significant changes in the crystal structure of TiO_2.

Nitrogen adsorption/desorption isotherms were measured using BET analysis to determine the specific surface area of graphite oxide, as well as of TiO_2 and the synthesized composite photocatalysts. Nitrogen adsorption/desorption isotherms of graphite oxide, TiO_2, as well as of TiO_2-rGO composites are shown in Fig. S1a and S1b in the Supplementary data, while the calculated BET specific surface areas are shown in Table 3. The BET specific surface area of graphite oxide and TiO_2 was 9.182 $m^2\,g^{-1}$ and 48.026 $m^2\,g^{-1}$, respectively, while the BET specific surface area of the synthesized composite photocatalysts TiO_2-rGO-HD and TiO_2-rGO-PH was 48.098 $m^2\,g^{-1}$ and 44.761 $m^2\,g^{-1}$, respectively. The overall shape of the adsorption/desorption isotherms for TiO_2-rGO composites indicates an adsorptive behaviour characteristic of macroporous materials or materials presenting low porosity.

Table 3
Calculated BET specific surface areas.

Sample	Specific surface area ($m^2\,g^{-1}$)
Graphite oxide	9.182
TiO_2 (Aeroxide P25)	48.026
TiO_2-rGO-HD	48.098
TiO_2-rGO-pH	44.761

Fig. 2a shows the Raman spectra of graphite and graphite oxide. As can be seen, the Raman spectrum of graphite is dominated by the characteristic G band at about 1580 cm^{-1} and the 2D band at about 2725 cm^{-1} [57]. The G band is a common feature of the Raman spectra of all sp^2 carbon forms and provides information on the in-plane vibration of sp^2 bonded carbon atoms. The small peak at about 1350 cm^{-1} (D band) suggests the presence of sp^3 defects and its intensity with respect to that of the G band is indicative of the crystalline quality [57], suggesting in our case the high quality of the precursor material. Higher order peaks of smaller intensity are also evident in the spectrum, such as the 2D band, which provides information on the stacking order of graphitic sp^2 materials. After oxidation, the Raman spectrum is characteristic of oxidized graphitic layers [58]. The Raman peaks of the spectrum of graphite oxide in Fig. 2b are fully consistent with the oxidation of the pristine graphite, featuring significant broadening and small blue shift of the G band peak, strong intensity enhancement of the D band rendering it comparable to the G band, and very broad and weak spectral features covering the 2D band region [58]. The fact that the intensity of the D band is comparable to the intensity of the G band suggests the presence of a high density of defects and structural disorder in the oxidized graphite oxide.

In addition, as can be seen in Fig. 2b, the Raman spectra of the composite photocatalysts TiO_2-rGO-HD and TiO_2-rGO-PH contain both the characteristic bands of TiO_2 in the region 100 cm^{-1}–700 cm^{-1}, as well as the characteristic bands D and E of graphene-based materials in the region 1300 cm^{-1}–1700 cm^{-1}. The fact that in the Raman spectra of TiO_2-rGO-HD and TiO_2-rGO-PH, the intensity of the D band is comparable to or higher than the intensity of the G band suggests the presence of defects and structural disorders in rGO, caused by TiO_2 anchored on the framework of rGO. More specifically, the I_D/I_G ratio of

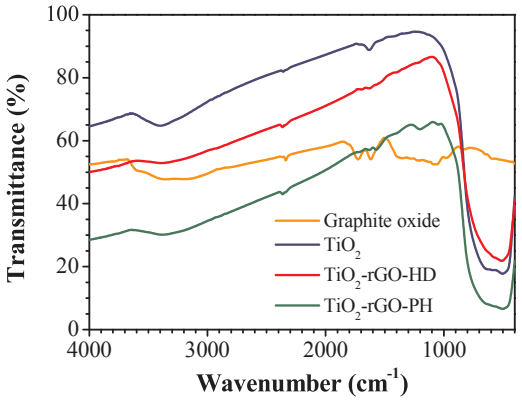

Fig. 3. FT-IR spectra of graphite oxide, TiO_2, TiO_2-rGO-HD and TiO_2-rGO-PH.

TiO_2-rGO-HD was 0.953 while for TiO_2-rGO-PH the I_D/I_G ratio was increased to 1.261. Increasing of the I_D/I_G ratio is attributed to the formation of more sp^3 defects in the carbon skeleton of rGO. From the above results, and based on Raman spectroscopy, it can be concluded that the composite photocatalyst TiO_2-rGO-HD has lower sp^3 defects in the carbon skeleton.

FT-IR spectra of graphite oxide, TiO_2, as well as of the synthesized composite photocatalysts TiO_2-rGO-HD and TiO_2-rGO-PH are shown in Fig. 3. As can be seen, the FT-IR spectrum of graphite oxide contains various characteristic absorption bands which correspond to various functional groups, such as hydroxyl (O—H, broad absorption band from 3000 cm^{-1} to 3700 cm^{-1} and centered at about 3250 cm^{-1}), carbonyl (C═O, strong absorption band peaked at about 1725 cm^{-1}), carbon-carbon double bond (C═C, strong absorption band peaked at about 1620 cm^{-1}), and carbon-oxygen single bonds (C—O, absorption bands at about 1210 cm^{-1} and 1040 cm^{-1}). On the other hand, in the FT-IR spectrum of TiO_2, the absorption peaks at about 3410 cm^{-1} and 1630 cm^{-1} correspond to the OH groups present on the surface of TiO_2, and the wide peak at about 400–900 cm^{-1} corresponds to the stretching vibration of the Ti—O—Ti bonds. After hydrothermal and photocatalytic treatment respectively, both synthesized composite photocatalysts, *i.e.* TiO_2-rGO-HD and TiO_2-rGO-PH, present a significant decrease in the intensity of all absorption peaks corresponding to oxygen functional groups, a fact that denotes the reduction of graphene oxide under these experimental conditions. In addition, the strong peaks at 400–900 cm^{-1} are attributed to the stretching vibration of Ti—O—Ti and possibly to Ti—O—C bonds.

Further characterization of graphite oxide, TiO_2, as well as of the synthesized composite photocatalysts TiO_2-rGO-HD and TiO_2-rGO-PH was performed by recording their X-ray photoelectron (XP) spectra. The survey scan revealed that the samples contain Ti, C and O as expected. Apart from the wide scan (data are not shown), core level peaks of C1s, Ti2p, and O1s were recorded, as shown in Fig. 4. More specifically, Fig. 4a shows the XP spectra of C1s peaks for graphite oxide, TiO_2-rGO-HD and TiO_2-rGO-PH. The binding energy of the main peak of TiO_2-rGO-HD and TiO_2-rGO-PH samples is at about 285.5 eV and is assigned to C—C, and C—H bonds, whereas for graphite oxide the spectra consist of two peaks at about 284.5 eV and 286.5 eV assigned to C—C, C—H and C—O, C—OH bonds. In addition, Fig. 4b shows the XP Spectra of Ti2p peak for bare TiO_2, as well as for TiO_2-rGO-HD and TiO_2-rGO-PH. The binding energy of the Ti2p peak indicates that Ti exists as titanium dioxide on all specimens' surfaces. Moreover, Fig. 4c shows the XP Spectra of O1s for graphite oxide, TiO_2, TiO_2-rGO-HD and TiO_2-rGO-PH. The O1s peak of the samples containing TiO_2 consists of two components; the first one at binding energy 530.2 ± 0.1 eV assigned to O in TiO_2, and the second one at binding energy at about 532.0 eV assigned to hydroxyls, carboxyls or adsorbed water. On the other hand, in the graphite oxide sample, the Ti-O component is not present, and the binding energy of the peak is centered at about 532.0 eV.

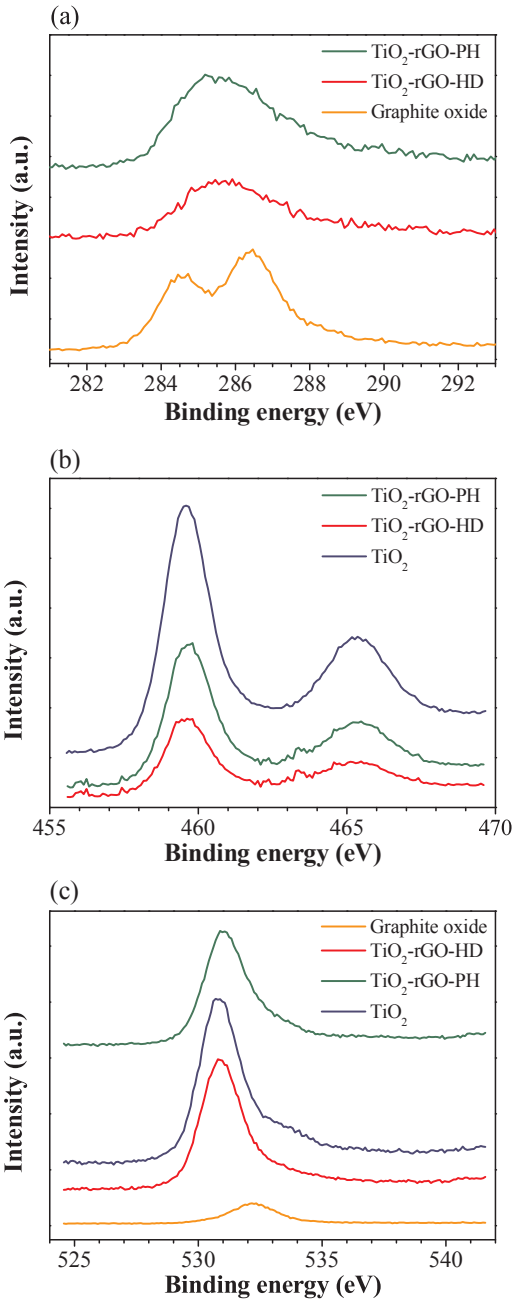

Fig. 4. X-ray photoelectron spectra of the core level peaks of: (a) C1s of graphite oxide, TiO_2-rGO-HD and TiO_2-rGO-PH; (b) Ti2p of TiO_2, TiO_2-rGO-HD and TiO_2-rGO-PH; and (c) O1s of graphite oxide, TiO_2, TiO_2-rGO-HD and TiO_2-rGO-PH.

Scanning Electron Microscopy (SEM) was used to observe the morphologies of graphite oxide, TiO_2, as well as of the synthesized TiO_2-rGO-HD and TiO_2-rGO-PH photocatalysts, and the obtained images are shown in Fig. 5. The morphology of each sample gives a visual understanding of its surface area structure, and of the possible ways to which the surface area may act as a site of adsorption or heterogeneous photocatalysis reactions. As can be seen in Fig. 5, the structure of the surface of each catalytic material is different, and the roughness varies in each material.

3.3. Degradation of antibiotics

The concentration of antibiotics in the MBR effluent in the dark (hydrolysis effect) and in the presence of simulated solar radiation (photolytic effect), in the absence of any photocatalytic particles, was

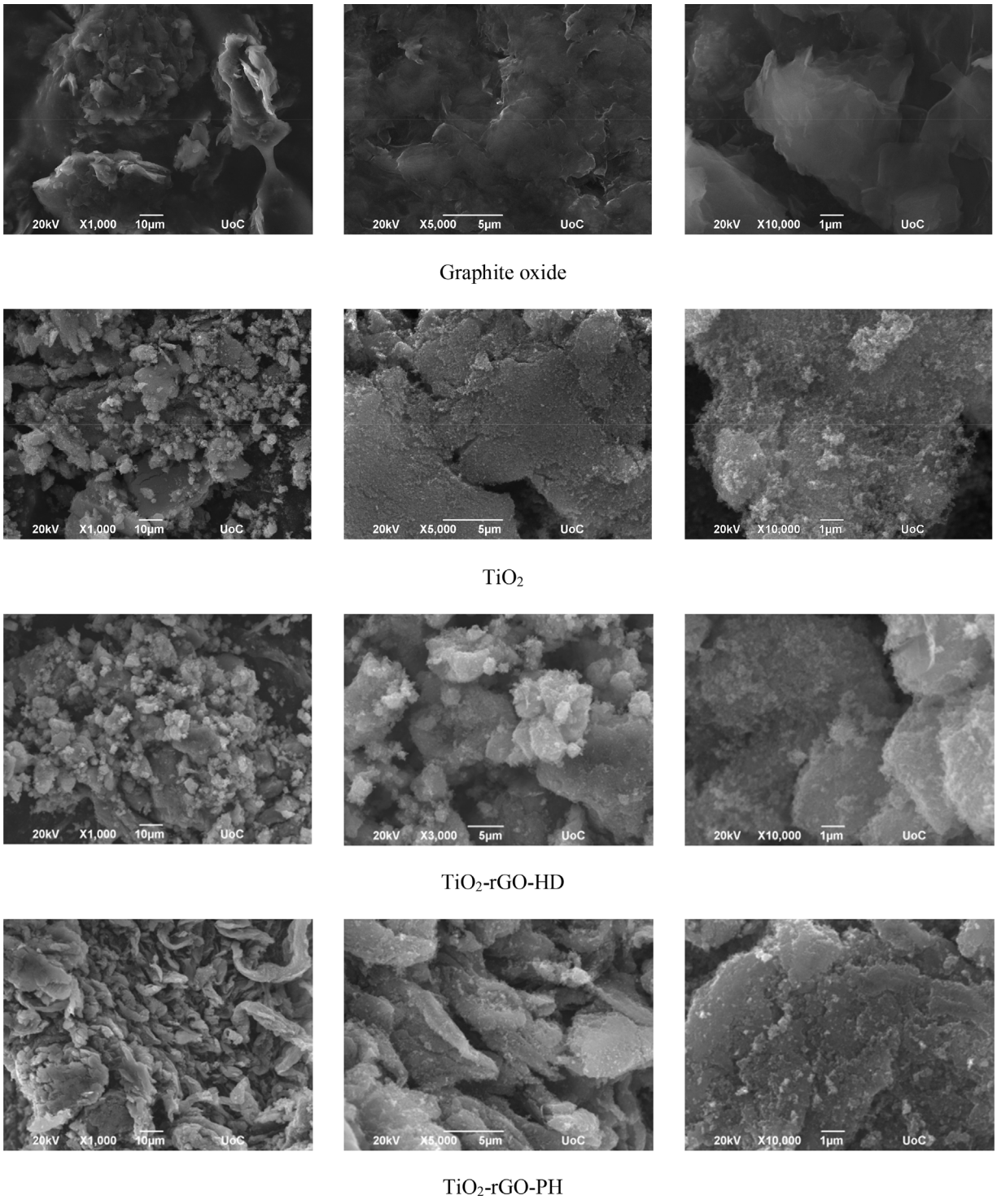

Fig. 5. SEM images of graphite oxide, TiO_2, TiO_2-rGO-HD and TiO_2-rGO-PH. Images on the left side are at the 10 μm scale, while images in the middle and on the right side are at the 5 μm and 1 μm scale, respectively.

initially investigated. The initial hydrolysis and photolysis experiments revealed an average total reduction of the three spiked antibiotics (C_0 = 100 μg L^{-1}) below 10(± 5)%.

Following, the potential of TiO_2 to adsorb the three examined antibiotics, in the dark (no catalyst photoactivation) was explored. In more detail, the adsorption of the three antibiotics onto the TiO_2 surface was examined for 30 min in the dark, before the beginning of the photocatalytic process. As can be seen in Table 4, the highest adsorption of CLA was achieved by TiO_2-rGO-PH, with 51(± 2)% reduction in

Table 4
Adsorption of the three antibiotics onto TiO_2, TiO_2-rGO-HD, and TiO_2-rGO-PH.

Adsorption and RSD (%)	TiO_2	TiO_2-rGO-PH	TiO_2-rGO-HD
CLA	9 ± 2	51 ± 2	3 ± 2
SMX	7 ± 1	31 ± 4	4 ± 1
ERY	7 ± 1	32 ± 3	20 ± 6

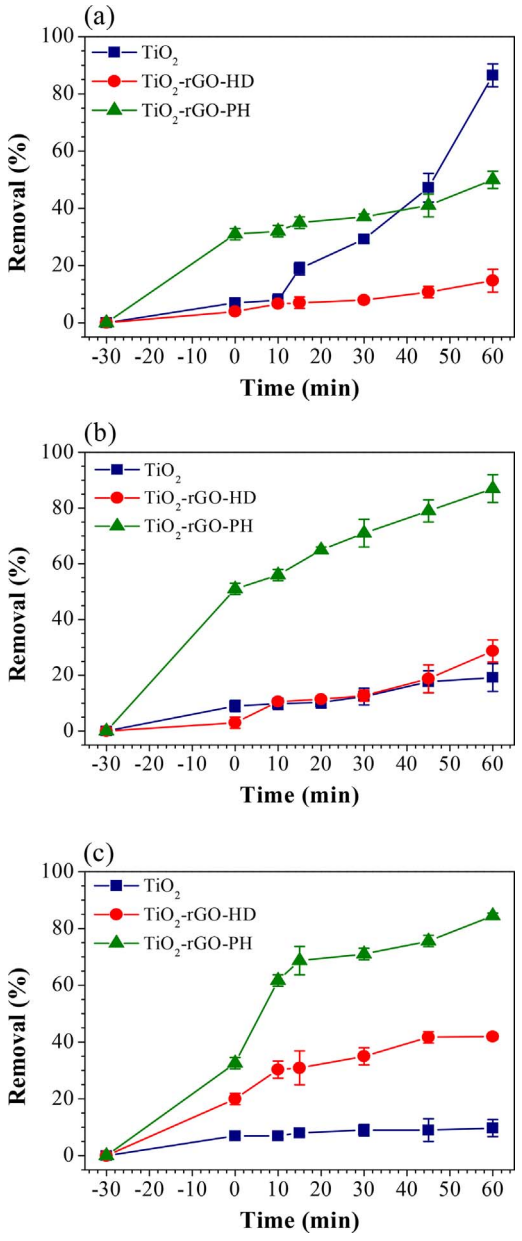

Fig. 6. Photocatalytic removal (%) of the antibiotics (a) SMX, (b) CLA, and (c) ERY over experimental time (min) with the three types of photocatalytic materials used (C_{cat} = 100 mg L^{-1}, V_{tot} = 300 mL).

concentration before the beginning of the photocatalytic treatment. Moreover, a 31(± 4)% and 32(± 3)% decrease were displayed by SMX and ERY respectively, on TiO_2-rGO-PH. Adsorption of the three antibiotics on TiO_2 and TiO_2-rGO-HD was lower (< 10%). The only exception to this observation was ERY, which exhibited a decrease in concentration in solution of 20(± 4)% in the presence of the TiO_2-rGO-HD composite.

Although the adsorption mechanism of pharmaceuticals onto graphene-based materials has not been completely deciphered yet [59], it has been shown so far that adsorption of organic compounds onto the surface of these materials is attributed to cation-π and π-π stacking interactions, as well as to electrostatic attractions [59]. This strong adsorption effect is suggested to be dominated by the polarization and electrostatic forces between cations and the permanent quadrupole of the π-electron-rich structures. These reactions are common between amino groups such as between the ones found in the three examined antibiotics, and π-electron-rich structures in TiO_2-rGO [59].

Next, the effect of photocatalytic treatment on the three antibiotics, spiked in the MBR effluent employing TiO_2, TiO_2-rGO-PH and TiO_2-rGO-HD, was examined. The removal efficiency of the three antibiotics by all studied photocatalytic materials used is shown in Fig. 6a–c. The photocatalytic trials using TiO_2 exhibited a removal of SMX of 87(± 4)% after 60 min of treatment. These results are in agreement with Hu et al. [60] who reported a complete SMX removal by TiO_2 under UVA irradiation. Moreover, a nearly complete mineralization of SMX was observed by Xekoukoulotakis et al. [61] and Abellán et al. [62] in TiO_2 aqueous suspensions under UVA irradiation.

The removal of ERY by TiO_2 was less efficient with only 10(± 3)% removal after 60 min of treatment under simulated solar irradiation. Xekoukoulotakis et al. [63] obtained a mineralization of ERY through the examination of the TOC content in an aqueous solution by 90%, while Vignesh et al. [64] also obtained a lower removal of ERY in an aqueous solution by TiO_2, with a removal of 31.6%.

CLA exhibited a similar photocatalytic degradation response in the presence of TiO_2 to the one shown by ERY, with 19(± 5)% total removal of the parent compound after 60 min of solar radiation. Overall, CLA is a highly hydrophobic compound with a high acidic stability [65], which may explain its highly recalcitrant character, making its removal through photocatalytic degradation difficult. This persistent behavior of the macrolide antibiotic can be attributed to its rather complex chemical structure. Indeed, CLA contains several functional groups, including various deactivating electron withdrawing groups, which may make electrophilic aromatic substitutions in organic compounds slower and more complicated [66].

The removal of the three examined antibiotics by heterogeneous photocatalysis in the presence of the novel synthesized TiO_2-rGO composites has been investigated next. As can be seen in Fig. 6, the overall removal of SMX by TiO_2-rGO-PH reached 50(± 3)% after 60 min irradiation, which is 37% lower than the corresponding removal obtained by TiO_2. Moreover, TiO_2-rGO-PH also achieved a 86(± 5)% and 84(± 2)% removal after 60 min irradiation for CLA and ERY, respectively. The TiO_2-rGO-PH removal potential was found to be higher than the one observed with TiO_2-rGO-HD, *i.e.*, removal of 29(± 4)% and 15(± 4)% for CLA and SMX, respectively, while ERY removal in the presence of TiO_2-rGO-HD was 42(± 1)%, which is half the performance of the TiO_2-rGO-PH photocatalyst.

The observed photocatalytic activity can be attributed to the strong interaction between TiO_2 and GO, which may facilitate the charge transfer from TiO_2 to graphene and hinder electron-hole recombination [19–24]. The electrons may further travel through the sp^2 hybridized network of the graphene towards oxygen groups to generate reactive oxygen species (ROS) which are involved in the chemical oxidation of organic microcontaminants [19–24]. As a result, the provision of open channels and an improved surface area of TiO_2-rGO composites may play an important role in the increased photocatalytic activity of the synthesized catalysts on the two examined macrolides [19–24]. As observed in Fig. 5, the structure of the catalyst surface after the TiO_2-rGO-HD and TiO_2-rGO-PH synthesis method has been altered, providing a transformed surface area on which photocatalytic reactions can take place, in comparison to TiO_2 surface. Overall, the synthesized TiO_2-rGO materials were shown to exceed the potential of commercially available TiO_2 as to the removal of CLA and ERY, two antibiotics which were proven to be recalcitrant compounds in wastewater treated with conventional biological processes [67,68].

3.4. Determination of inactivation profile of total E. coli during photocatalytic treatment

In further experiments, the inactivation of total spiked *E. coli* in the presence of the photocatalysts under simulated solar radiation was studied. Experiments were conducted in the MBR effluent, which was not spiked with any antibiotics, in order to determine the effect of the photocatalytic treatment alone on the survival/inactivation of the total

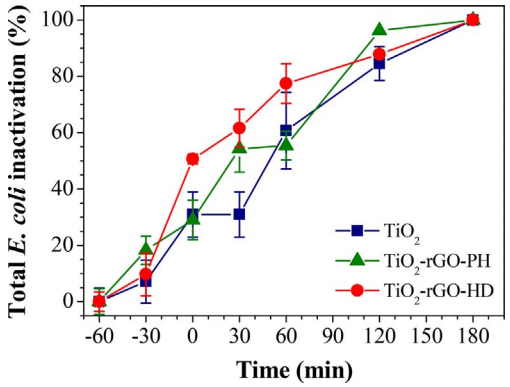

Fig. 7. The inactivation of total *E. coli* (%) by heterogeneous photocatalysis over experimental time (min) with the three examined catalysts, in MBR treated effluent (C_{cat} = 100 mg L^{-1}, V_{tot} = 300 mL).

spiked bacteria. The aliquot samples were plated on agar that did not contain any antibiotics, to non-selectively grow all *E. coli* and enumerate the total population, including both antibiotic-susceptible and ARB.

Preliminary inactivation experiments in the dark and under simulated radiation for 180 min were carried out in the absence of the catalyst. The results have shown a decrease in the order of less than 1 log of CFU mL^{-1} of total bacteria, both in the dark and under simulated solar radiation.

The results of the inactivation of total *E. coli* in the presence of the examined catalysts are shown in Fig. 7. The first 60 min of magnetic stirring in the dark of the MBR effluent inoculated with TiO_2 or TiO_2-rGO-PH and the bacteria, resulted in an average percentage reduction in the CFU concentration of *E. coli*, of less than 31(± 8)%. The cause of the reduction may be attributed to the adsorption of catalyst particles onto bacteria, or to the physical damage caused by the direct contact of the catalyst with the bacteria, leading to their inactivation and loss of cultivability. The inactivation of *E. coli* in the presence of these catalysts was less efficient than in the presence of TiO_2-rGO-HD in the dark, as this material had a more marked impact on the survival of *E. coli*, with a reduction in visible colonies on media of 51(± 2)%. This difference in efficiency may be attributed to catalyst structure morphology, which may cause increased physical damage to the total *E. coli* population found in the solution. Furthermore, the sensitivity of the indigenous *E. coli* to the presence of catalytic particles even in the dark, indicates their physical vulnerability to cell wall and cell membrane damages, which may consequently lead to rupturing of the cell wall/membrane and allow leakage of cell components to the external environment [69,70].

After illumination with simulated solar radiation of the aqueous slurries containing suspensions of *E. coli* and the photocatalysts, the inactivation of *E. coli* exhibited an increase compared to its inactivation percentage in the dark. After 180 min of radiation, all three photocatalysts achieved a complete absence of cultivable colonies on the growth media (< LOD). The high inactivation after 180 min of treatment indicates the significant impact that the photocatalytic oxidation can have on cellular functions and structures, rendering cells inactive or killing them altogether. It should be noted that the impact of all photocatalysts on total *E. coli* is pronounced both in the dark and under simulated solar radiation. This finding highlights the important contribution of the adsorption of photocatalytic particles on bacteria and of the physical cell damage exerted by the photocatalysts (both processes taking place in the dark and under illumination) to the overall bacterial inactivation observed (29%–51% for all three examined photocatalysts in the dark, followed by 100% inactivation under simulated solar radiation). The pronounced effect of all three photocatalytic materials on bacterial cells further suggests that the damage to cells, both reversible or irreversible, may be leading to loss of growth ability of the damaged cells on the cultivation media used [71].

Foster et al. [72] proposed a sequence of events that may take place in order to inactivate/render non-viable a bacterial cell during photocatalysis with TiO_2. The authors suggested that the initial contact of bacteria with catalyst particles leading to particle binding onto cells may cause damage to the bacterial cell wall revealing the inner cell membrane. Next, the cell membrane also may get physically injured or rupture, releasing cell contents and allowing catalyst particles to enter the cell and produce further physical damage while hindering vital metabolic and physiological processes inside the cell. At this point, the damage is reversible and may be corrected if the cells are not exposed to other sources of stress. The photocatalytic treatment also produces reactive oxygen species (ROS) such as O_2· and HO·, which are the main influencing factors in the subsequent inactivation of the damaged cells, because they may confer cell membrane/cell wall modifications, as well as inner cell component damage and modifications [73–76]. Exposed cell component oxidation through the production of ROS, may take place once there is direct cell-catalyst contact [77]. On the other hand, produced ROS have the capacity of cell component damage in close distance from the catalyst particles, thus not only affecting cells in direct contact with catalyst particles but also in close proximity to them [78].

The cellular effect of various graphene-based materials has been demonstrated by Liu et al. [79], where GO and rGO were examined as to their antibacterial activity. The results of the study showed a higher loss of *E. coli* viability by GO than by rGO, with the biggest fraction of cell inactivation occurring in the first hour of treatment. In another study by Fernández-Ibáñez et al. [14], TiO_2-rGO composites synthesized using the photocatalytic reduction of exfoliated GO by TiO_2 under UV radiation, were used to disinfect water contaminated with *E. coli* and *Fusarium solani* spores under real sunlight. Moreover, the production of singlet oxygen was measured using fluorescence intensity of a singlet oxygen specific fluorophore, relative to a control sample of distilled water. An enhancement in the rate of *E. coli* inactivation was observed compared to TiO_2, while the rate of inactivation of the *Fusarium solani* spores remained the same for both catalysts examined. In another study by the same authors [29], it was found using probes, that the main ROS involved in the TiO_2-rGO photocatalytic disinfection of *E. coli*, were determined to be hydrogen peroxide, HO· and O_2· under UV–vis radiation, while only O_2· was found under visible radiation.

3.5. Development of the prevalence profile of antibiotic-resistant E. coli during photocatalytic treatment

The developed profile of antibiotic-resistant *E. coli* during photocatalytic treatment (Fig. 8a–c) have been analysed, in order to observe potential trends in photocatalytic inactivation, that may be associated to the resistance of the bacteria to a specific antibiotic.

The most pronounced effect of the catalyst particles alone on *E. coli*, after 60 min of bacterial exposure in the dark, was shown in the case of TiO_2 (*i.e.* 75(± 7)% reduction in ERY-resistant *E. coli* and 39(± 6)% reduction in SMX-resistant *E. coli*). This finding indicates the increased adsorption effect or susceptibility of antibiotic-resistant *E. coli* to cellular damage and loss of cultivability in the presence of the photocatalysts, due to physical damage occurring on the cell surface due to contact with photocatalyst particles.

Additionally, it was seen in this study that the cultivability of ERY- and SMX-resistant bacteria was lost in the dark, even before the photocatalysis began. Sub-lethal concentrations of a stressor, such as the concentration of the antibiotic, in combination to the exposure to suspended catalyst particles, may have produced added environmental stress that may lead to the induction of a VBNC state in the bacteria [51]. The subsequent repair and re-activation of bacteria therefore is an important parameter to be investigated when dealing with processes that may put bacteria in such a VBNC state, to ensure that the damage caused is leading to permanent inactivation, and not to the post-treatment re-growth of bacteria.

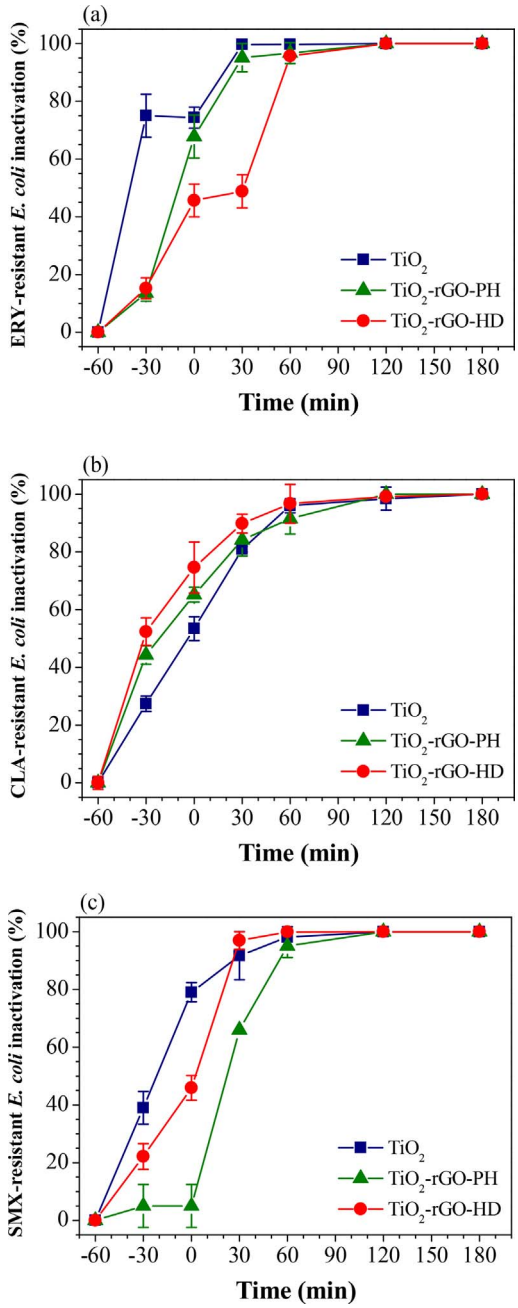

Fig. 8. The inactivation (%) of antibiotic-resistant *E. coli* throughout the photocatalytic treatment (min) for (a) ERY-resistant *E. coli*, (b) CLA-resistant *E. coli* and (c) SMX-resistant *E. coli* (C_{cat} = 100 mg L^{-1}, V_{tot} = 300 mL).

As the photocatalytic treatment began and the photocatalytic oxidation reactions were initiated, the most rapid inactivation of antibiotic-resistant *E. coli* was observed in the presence of ERY, as TiO_2 achieved its complete inactivation after 30 min of treatment. ERY-resistant *E. coli* bacteria were not visible on the selective media after 120 min of treatment in the presence of all photocatalysts while the inactivation of CLA- and SMX-resistant *E. coli* followed a similar pattern. It is suggested from this finding that the efficient inactivation of antibiotic-resistant *E. coli* to all examined antibiotics, shows that AR mechanisms do not also provide cellular protection in the presence of photocatalytically produced ROS, or protection mechanisms to resist physical damage.

Overall, there was a high variation in the development of the AR profiles and in the post-treatment regrowth potential of both examined types of bacteria, which changed according to the combination of treatment-antibiotic present. This observation may also indicate variation in the genetic profiles of the autochthonous community of *E. coli* that was isolated from real wastewater, and was used for the photocatalytic experiments. The variability in AR profiles of the bacteria used also reflects the real-life scenario, as a large range of phenotypic as well as genotypic profiles exists in real wastewater matrices.

There is limited research regarding the effect of heterogeneous TiO_2 photocatalysis, and especially of newly synthesized photocatalytic materials such as graphene and its derivative composites such as TiO_2-rGO, to support and explain the above findings. The research conducted so far, regards a limited number of bacterial species. According to Tsai et al. [77], altered susceptibility to TiO_2 photocatalysis may come about through the mutation of genes involved in the ROS resistance. In addition to cellular mechanisms to resist ROS damage, ARB may present altered resistance to photocatalytic treatment through gene regulation and stepwise gene mutation acquisition, such as plasmid-mediated HGT. This process may equip bacteria with genetic material, which can combine resistance to photocatalytic treatment and to antibiotics [80]. Moreover, the reduced antibiotic susceptibility of Gram-negative bacteria which include *E. coli,* compared to antibiotic-positive bacteria has also been previously attributed to outer cellular component alteration/destruction. More specifically, these components involve cell wall structures which include additional structural barriers such as lipopolysaccharides to the entry of inhibitory or harmful substances, as well as to their ability to produce catalase enzymes, which limit the formation of ROS during photocatalytic treatment [81].

3.6. Regrowth potential of *E. coli* after the end of the photocatalytic treatment

Even though the ability of bacteria to grow in cultivation media may be lost after photocatalytic treatment, the potential of their repair and regrowth, given the necessary recuperation time, should not be neglected, as this phenomenon was shown to take place in various studies examining the disinfection potential of various heterogeneous photocatalysts [15,82]. Therefore, the regrowth potential of *E. coli* at different experimental times was studied thereafter during photocatalysis in order to establish the experimental time which is capable of permanently inactivating *E. coli*, thus avoiding the re-activation and regrowth of the bacteria during storage of the treated effluent. All photocatalysis experimental times were examined in this study, in order to observe their inactivating capacity (counts of bacterial colonies immediately after treatment), compared to the regrowth potential generated at each experimental time (counts of bacterial colonies after 24 h of storage). Samples for regrowth examination were incubated at 37 °C for 24 h in the dark, and then plated on TSA agar. The ratio of the enumerated colonies (CFU mL^{-1}) in the incubated samples after 24 h of storage (C_r) to the colonies enumerated in the obtained samples at the time of treatment (C_t) was calculated, and expressed as C_r/C_t.

Fig. 9 shows the findings of the regrowth study done on *E. coli* after photocatalytic treatment, at different experimental times. The results have shown a considerable regrowth of *E. coli* during the dark treatment, in the presence of the photocatalytic particles, despite the original reduction in colony counts due to physical cell damage. More specifically, a C_r/C_t ratio of 6 was found for Aeroxide P25 TiO_2 and TiO_2-rGO-PH, signifying the growth on solid media, of higher counts of *E. coli* by 6 orders of magnitude after 24 h of storage, than the ones found in the plated samples just after treatment. The same phenomenon was observed until the time that the solar simulator was turned on, and the photocatalytic process began. In contrast, treatment with TiO_2-rGO-HD, achieved a reduced bacterial regrowth during the first 60 min of dark treatment compared to the other two photocatalysts (C_r/C_t ratio of 3). This finding may suggest that the physical contact and bacterial surface damage incurred by TiO_2-rGO-HD may produce a more severe and permanent inactivation effect on bacteria, thus reducing the counts of *E. coli* that are thereafter cultivable on solid media.

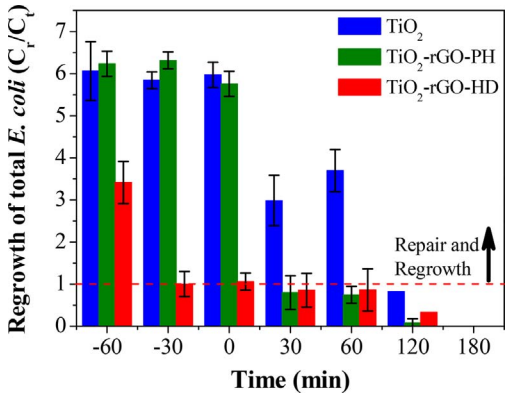

Fig. 9. The regrowth of total *E. coli* bacteria after incubation of treated samples at different experimental times at 37 °C for 24 h. The dotted line signifies the photocatalytic disinfection achieved reduction in *E. coli*. All bars above this limit indicate regrowth numbers (CFU mL^{-1}) above the observed results during the photocatalytic experiments. C_r/C_t is the average CFU mL^{-1} after 24 h of incubation (regrowth), divided by the average observed result during the photocatalytic experiments, from 3 replicate experiments (C_{cat} = 100 mg L^{-1}, V_{tot} = 300 mL).

On the other hand, as can be seen in Fig. 9, the photocatalytic treatment has achieved a reduced regrowth effect on *E. coli*. More specifically, the only C_r/C_t ratio that exceeded 1 was observed in the presence of TiO_2 at experimental times of 30 and 60 min (C_r/C_t ratio of 3 and 3.7 respectively). The other two photocatalytic materials achieved a reduction in bacterial counts, below a C_r/C_t ratio of 1. The most significant observation however, is that after 180 min of photocatalytic treatment, all three photocatalytic materials achieved a complete inactivation of *E. coli*, as no visible colonies were grown on the selective media. This result indicates the efficiency of photocatalytic oxidation in the permanent inactivation of *E. coli*. However, it was revealed that experimental treatment time also plays a significant role in the permanent inactivation of bacteria. The longer the treatment time, the more significant the inactivation effect exhibited on bacteria [83]. This indicates that, at the experimental conditions employed in the present work, 180 min is adequate treatment time to prevent regrowth of *E. coli*, even 24 h after treatment. However, it should be noted that in real-case wastewater treatment settings, the conclusions regarding the optimum time for complete absence of regrowth would vary, according to system volume, particle concentration and solar exposure time, amongst others.

3.7. Effect of photocatalysis on total DNA content

The total DNA content of samples was examined after photocatalysis in MBR effluent. The results are shown in Fig. 10. As can be seen, the total genomic DNA concentration was not affected by the treatment, as the concentration remained steady with less than 10% change even after 60 min of photocatalysis. The genomic DNA concentration of the MBR effluent (4.7 ng μL^{-1}, ± 6%) was not reduced by photocatalytic oxidation even though the total bacterial counts and the prevalence of ARB were influenced by the type of photocatalytic treatment (Sections 3.4 and 3.5). The total DNA content of the MBR effluent, treated with activated sludge, contains the genetic material contained intra- and extra-cellularly, and reflects the rich genetic diversity originating from the mixture of activated sludge acting on the micropollutants, with the incoming wastewater inside the reactor. The physically filtered MBR effluent contains a low concentration of total DNA, which may contain genetic material resistant to photocatalytic oxidation and to potential physical damage by catalyst particles. The potential genetic constituents of the genomic DNA may include genes conferring resistance to antibiotics and other antimicrobials, among others. As a result, to examine the molecular constitution of the remaining genomic DNA before and after photocatalytic treatment, the relative quantification of selected ARGs and species-specific genes took place next.

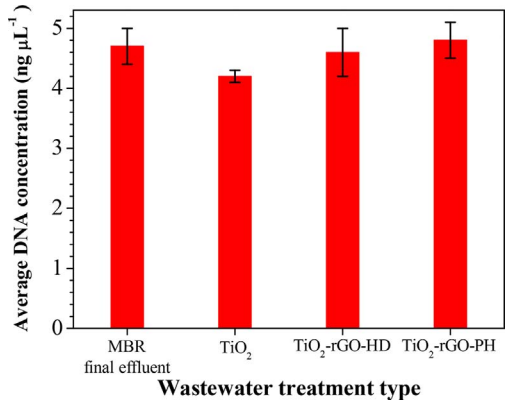

Fig. 10. The average DNA concentration (ng) in each µL of sample examined (C_{cat} = 100 mg L^{-1}, V_{tot} = 300 mL).

3.8. Development of species-specific genes and ARGs profiles

The prevalence of the selected ARGs (*amp*C, *sul*1, *erm*B) and species-specific sequences (*ecf*X, enterococcal 23S rRNA) was examined after photocatalytic treatment with the examined catalysts in the MBR effluent. The estimated $\log_{10}$ cell equivalents (CE) 100 ng^{-1} DNA in the examined samples during photocatalytic treatment for a total of 180 min are given in Fig. 11.

As can be seen, enterococci analysed with the 23S rRNA primer system was the most prevalent genetic sequence detected in all samples examined, (3.52–3.95 $\log_{10}$ CE 100 ng^{-1} DNA), suggesting that their removal is more challenging compared to the removal of the other sequences examined. TiO_2 photocatalytic treatment displayed no reduction of *P. aeruginosa* (*ecf*X) (0.55–1.14 $\log_{10}$ CE 100 ng^{-1} DNA), but the photocatalytic treatment with TiO_2-rGO-PH and TiO_2-rGO-HD successfully reduced *P. aeruginosa* in the respective wastewater effluent, thus indicating a sensitivity of the target organism to photocatalytic oxidation with the latter two synthesized photocatalysts, but not with pristine TiO_2.

*Sul*1 (sulfonamide resistance gene) is abundant after 60 min of treatment with TiO_2, TiO_2-rGO-PH and TiO_2-rGO-HD photocatalysts (2.37–2.92 $\log_{10}$ CE 100 ng^{-1} DNA), thus indicating that the bacterial carrier of the mentioned ARGs was relatively stable under photocatalytic treatment. *Amp*C (ampicillin resistance gene) abundance did not change after treatment with TiO_2, but this specific gene encoding resistance to β-lactams was not detected in samples treated with TiO_2-

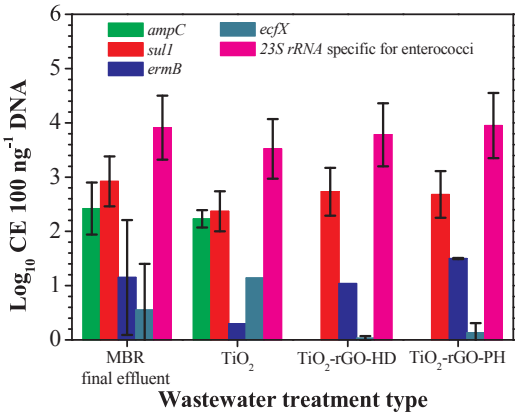

Fig. 11. The $\log_{10}$ abundance of the examined genetic parameters in the photocatalytically treated MBR effluent with the examined catalysts. Mean values are represented in $\log_{10}$ cell equivalent (CE) values per 100 ng of DNA (C_{cat} = 100 mg L^{-1}, V_{tot} = 300 mL).

rGO-PH and TiO_2-rGO-HD, indicating the superiority of the latter two photocatalysts in the removal of such resistant bacteria carrying the *amp*C gene. The erythromycin resistance gene *erm*B was also found in the MBR effluent (1.2. $\log_{10}$ CE 100 ng^{-1} DNA). The photocatalytic treatment achieved a 4-fold reduction in its prevalence after treatment (0.3 $\log_{10}$ CE 100 ng^{-1} DNA) with TiO_2 but it did not influence this target organism after treatment with TiO_2-rGO-HD and TiO_2-rGO-PH. The *mec*A gene was not detected in any of the samples examined.

The reduction in the abundance of *amp*C and *ecf*X can be attributed to intracellular DNA damages of bacteria produced by photo-irradiated TiO_2-rGO and TiO_2 particles. According to Hirakawa et al. [81], photocatalytic treatment causes the breakdown of long DNA strands to shorter oligonucleotides, indicating the breakage of the deoxyribose phosphate backbone. Moreover, the authors suggest that DNA damage by photocatalytic treatment occurs at specific sites on the DNA double strand causing its photo-cleavage and causing base modifications, producing mutations in the offspring [82].

4. Conclusions

The conclusions drawn from the present study can be summarized as follows:

- The synthesized photocatalysts were capable of removing the target antibiotics in real wastewater effluents under simulated solar radiation. TiO_2-rGO-PH outperformed TiO_2 and TiO_2-rGO-HD as to the removal of CLA and ERY, but TiO_2 was found to be the most efficient photocatalyst for the removal of SMX.
- Complete inactivation of *E. coli* after 180 min was exhibited with all examined photocatalysts, and antibiotic-resistant *E. coli* did not follow a particular inactivation trend, as each photocatalyst achieved a different inactivation pattern of *E. coli* resistant to each antibiotic.
- As treatment time increased, the cultivable *E. coli* counts decreased, and regrowth potential of the bacteria decreased, while it was shown that 180 min of photocatalytic treatment was adequate for the complete and non-reversible inactivation of *E. coli*, even after 24 h of post-treatment storage.
- The least amount of regrowth at all experimental times was observed in the presence of TiO_2-rGO-HD, thus indicating its superiority to the other examined photocatalysts as regards permanent inactivation of bacteria leading to lack of repair/reactivation during storage of treated wastewater effluents.
- The examined genes, both species-specific and ARGs contained within these treated samples, did not all behave similarly during photocatalytic treatment, as specific genes were degraded, while others, such as *sul*1, *ermB* resistance genes, and enterococci detected *via* the 23S rRNA gene sequences, were persistent throughout the treatment.
- The existence of bacterial defense mechanisms against ROS-induced cellular damage may play an important part in the disinfection of both total and antibiotic-resistant *E. coli*, and this needs to be further investigated for the optimum disinfecting application of TiO_2-rGO photocatalysis. Moreover, more studies are required in real wastewater effluents to determine the potential of graphene-based photocatalysts in the overall decontamination and disinfection of highly complex matrices, such as urban wastewaters.

Overall, it was shown through this study that the composition of the heterogeneous photocatalytic materials utilized has the potential to play an important role in the decontamination of wastewater from a mixture of antibiotic compounds, and disinfect such matrices from pathogenic bacteria and ARB. Of course, more studies are required in real wastewater to determine the potential of such materials in the overall decontamination and disinfection of highly complex matrices, such as urban wastewater. Finally, a complete and permanent inactivation of ARB and the maximum removal of ARGs should be achieved to minimize the risk of antibiotic resistance spread into the receiving waters.

Acknowledgements

This work was co-funded by the Republic of Cyprus and the European Regional Development Fund through grant AEIFOPIA/ΦΥΣΗ/0311(BIE)/33 (PhotoGraph) through the Cyprus Research Promotion Foundation (DESMI 2009–2010). The authors would also like to acknowledge the COST Action ES1403 NEREUS "New and emerging challenges and opportunities in wastewater reuse", supported by COST (European Cooperation in Science and Technology, www.cost.eu) for enabling the collaboration among the authors of the paper. Nireas-IWRC (NEA ΥΠΟΔΟΜΗ/ΣΤΡΑΤΗ/0308/09) was co-financed by the Republic of Cyprus and the European Regional Development Fund through the Research Promotion Foundation of Cyprus.

Appendix A. Supplementary data

Supplementary data associated with this article can be found, in the online version, at http://dx.doi.org/10.1016/j.apcatb.2017.11.020.

References

[1] UN-Water: Annual Report 2015, Geneve, Switzerland. < http://www.unwater.org/publications/publications-detail/en/c/428244// > , 2015 (Accessed 2 February 2017).
[2] L. Rizzo, C. Manaia, C. Merlin, T. Schwartz, C. Dagot, M.C. Ploy, I. Michael, D. Fatta-Kassinos, Urban wastewater treatment plants as hotspots for antibiotic resistant bacteria and genes spread into the environment: a review, Sci. Total Environ. 447 (2013) 345–360, http://dx.doi.org/10.1016/j.scitotenv.2013.01.032.
[3] T.U. Berendonk, C.M. Manaia, C. Merlin, D. Fatta-Kassinos, E. Cytryn, F. Walsh, H. Bürgmann, H. Sørum, M. Norström, M.-N. Pons, N. Kreuzinger, P. Huovinen, S. Stefani, T. Schwartz, V. Kisand, F. Baquero, J.L. Martinez, Tackling antibiotic resistance: the environmental framework, Nat. Rev. Microbiol. 13 (2015) 310–317, http://dx.doi.org/10.1038/nrmicro3439.
[4] H.K. Allen, J. Donato, H.H. Wang, K.A. Cloud-Hansen, J. Davies, J. Handelsman, Call of the wild: antibiotic resistance genes in natural environments, Nat. Rev. Microbiol. 8 (2010) 251–259, http://dx.doi.org/10.1038/nrmicro2312.
[5] Y. Pachepsky, J. Morrow, A. Guber, D. Shelton, R. Rowland, G. Davies, Effect of biofilm in irrigation pipes on microbial quality of irrigation water, Lett. Appl. Microbiol. 54 (2012) 217–224, http://dx.doi.org/10.1111/j.1472-765X.2011.03192.x.
[6] N. Al-Jassim, M.I. Ansari, M. Harb, P.Y. Hong, Removal of bacterial contaminants and antibiotic resistance genes by conventional wastewater treatment processes in Saudi Arabia: is the treated wastewater safe to reuse for agricultural irrigation? Water Res. 73 (2015) 277–290, http://dx.doi.org/10.1016/j.watres.2015.01.036.
[7] S. Yomoda, T. Okubo, A. Takahashi, M. Murakami, S. Iyobe, Presence of *Pseudomonas putida* strains harboring plasmids bearing the metallo-β-lactamase gene *bla*IMP in a hospital in Japan, J. Clin. Microbiol. 41 (2003) 4246–4251, http://dx.doi.org/10.1128/JCM.41.9.4246-4251.2003.
[8] T. Schwartz, W. Kohnen, B. Jansen, U. Obst, Detection of antibiotic-resistant bacteria and their resistance genes in wastewater, surface water, and drinking water biofilms, FEMS Microbiol. Ecol. 43 (2003) 325–335, http://dx.doi.org/10.1111/j.1574-6941.2003.tb01073.x.
[9] V. Gomez-Alvarez, R.P. Revetta, J.W. Santo Domingo, Metagenomic analyses of drinking water receiving different disinfection treatments, Appl. Environ. Microbiol. 78 (2012) 6095–6102, http://dx.doi.org/10.1128/AEM.01018-12.
[10] C. Bouki, D. Venieri, E. Diamadopoulos, Detection and fate of antibiotic resistant bacteria in wastewater treatment plants: a review, Ecotoxicol. Environ. Saf. 91 (2013) 1–9, http://dx.doi.org/10.1016/j.ecoenv.2013.01.016.
[11] M. Munir, I. Xagoraraki, Levels of antibiotic resistance genes in manure, biosolids, and fertilized soil, J. Environ. Qual. 40 (2011) 248, http://dx.doi.org/10.2134/jeq2010.0209.
[12] J. Alexander, G. Knopp, A. Dötsch, A. Wieland, T. Schwartz, Ozone treatment of conditioned wastewater selects antibiotic resistance genes, opportunistic bacteria, and induce strong population shifts, Sci. Total Environ. 559 (2016) 103–112, http://dx.doi.org/10.1016/j.scitotenv.2016.03.154.
[13] D.M.A. Alrousan, M.I. Polo-López, P.S.M. Dunlop, P. Fernández-Ibáñez, J.A. Byrne, Solar photocatalytic disinfection of water with immobilised titanium dioxide in recirculating flow CPC reactors, Appl. Catal. B Environ. 128 (2012) 126–134, http://dx.doi.org/10.1016/j.apcatb.2012.07.038.
[14] P. Fernández-Ibáñez, M.I. Polo-López, S. Malato, S. Wadhwa, J.W.J. Hamilton, P.S.M. Dunlop, R. D'Sa, E. Magee, K. O'Shea, D.D. Dionysiou, J.A. Byrne, Solar photocatalytic disinfection of water using titanium dioxide graphene composites, Chem. Eng. J. 261 (2015) 36–44, http://dx.doi.org/10.1016/j.cej.2014.06.089.
[15] C.H.A. Tsang, H.Y.H. Kwok, Z. Cheng, D.Y.C. Leung, The applications of graphene-

based materials in pollutant control and disinfection, Prog. Solid State Chem. 45 (2017) 1–8, http://dx.doi.org/10.1016/j.progsolidstchem.2017.02.001.
[16] W. Wang, G. Li, D. Xia, T. An, H. Zhao, P.K. Wong, Photocatalytic nanomaterials for solar-driven bacterial inactivation: recent progress and challenges, Environ. Sci. Nano 4 (2017) 782–799, http://dx.doi.org/10.1039/C7EN00063D.
[17] P.V.L. Reddy, B. Kavitha, P.A.K. Reddy, K.-H. Kim, TiO_2-based photocatalytic disinfection of microbes in aqueous media: a review, Environ. Res. 154 (2017) 296–303, http://dx.doi.org/10.1016/j.envres.2017.01.018.
[18] W. Wang, G. Huang, J.C. Yu, P.K. Wong, Advances in photocatalytic disinfection of bacteria: development of photocatalysts and mechanisms, J. Environ. Sci. 34 (2015) 232–247, http://dx.doi.org/10.1016/j.jes.2015.05.003.
[19] M. Faraldos, A. Bahamonde, Environmental applications of titania-graphene photocatalysts, Catal. Today 285 (2017) 13–28, http://dx.doi.org/10.1016/j.cattod.2017.01.029.
[20] V. Kumar, K.-H. Kim, J.-W. Park, J. Hong, S. Kumar, Graphene and its nanocomposites as a platform for environmental applications, Chem. Eng. J. 315 (2017) 210–232, http://dx.doi.org/10.1016/j.cej.2017.01.008.
[21] N. Zhang, M.-Q. Yang, S. Liu, Y. Sun, Y.-J. Xu, Waltzing with the versatile platform of graphene to synthesize composite photocatalysts, Chem. Rev. 115 (2015) 10307–10377, http://dx.doi.org/10.1021/acs.chemrev.5b00267.
[22] R.K. Upadhyay, N. Soin, S.S. Roy, Role of graphene/metal oxide composites as photocatalysts, adsorbents and disinfectants in water treatment: a review, RSC Adv. 4 (2014) 3823–3851, http://dx.doi.org/10.1039/C3RA45013A.
[23] X. Huang, X. Qi, F. Boey, H. Zhang, Graphene-based composites, Chem. Soc. Rev. 41 (2012) 666–686, http://dx.doi.org/10.1039/c1cs15078b.
[24] Q. Xiang, J. Yu, M. Jaroniec, Graphene-based semiconductor photocatalysts, Chem. Soc. Rev. 41 (2012) 782–796, http://dx.doi.org/10.1039/c1cs15172j.
[25] S. Eigler, A. Hirsch, Chemistry with graphene and graphene oxide-challenges for synthetic chemists, Angew. Chem. Int. Ed. Engl. 53 (2014) 7720–7738, http://dx.doi.org/10.1002/anie.201402780.
[26] K.S. Novoselov, A.K. Geim, S.V. Morozov, D. Jiang, Y. Zhang, S.V. Dubonos, I.V. Grigorieva, A.A. Firsov, Electric field effect in atomically thin carbon films, Science 306 (2004) 666–669, http://dx.doi.org/10.1126/science.1102896.
[27] A.K. Geim, K.S. Novoselov, The rise of graphene, Nat. Mater. 6 (2007) 183–191, http://dx.doi.org/10.1038/nmat1849.
[28] X. Zeng, Z. Wang, N. Meng, D.T. McCarthy, A. Deletic, J. Pan, X. Zhang, Highly dispersed TiO_2 nanocrystals and carbon dots on reduced graphene oxide: ternary nanocomposites for accelerated photocatalytic water disinfection, Appl. Catal. B Environ. 202 (2017) 33–41, http://dx.doi.org/10.1016/j.apcatb.2016.09.014.
[29] B.R. Cruz-Ortiz, J.W.J. Hamilton, C. Pablos, L. Díaz-Jiménez, D.A. Cortés-Hernández, P.K. Sharma, M. Castro-Alférez, P. Fernández-Ibañez, P.S.M. Dunlop, J.A. Byrne, Mechanism of photocatalytic disinfection using titania-graphene composites under UV and visible irradiation, Chem. Eng. J. 316 (2017) 179–186, http://dx.doi.org/10.1016/j.cej.2017.01.094.
[30] L.-P. Liu, X.-N. Yang, L. Ye, D.-D. Xue, M. Liu, S.-R. Jia, Y. Hou, L.-Q. Chu, C. Zhong, Preparation and characterization of a photocatalytic antibacterial material: graphene oxide/TiO_2/bacterial cellulose nanocomposite, Carbohydr. Polym. 174 (2017) 1078–1086, http://dx.doi.org/10.1016/j.carbpol.2017.07.042.
[31] G. Wang, W. Feng, X. Zeng, Z. Wang, C. Feng, D.T. McCarthy, A. Deletic, X. Zhang, Highly recoverable TiO_2–GO nanocomposites for stormwater disinfection, Water Res. 94 (2016) 363–370, http://dx.doi.org/10.1016/j.watres.2016.02.067.
[32] M.D. Rojas-Andrade, G. Chata, D. Rouholiman, J. Liu, C. Saltikov, S. Chen, Antibacterial mechanisms of graphene-based composite nanomaterials, Nanoscale 9 (2017) 994–1006, http://dx.doi.org/10.1039/C6NR08733G.
[33] J. Zhu, J. Wang, J. Hou, Y. Zhang, J. Liu, B. der Bruggen, Graphene-based antimicrobial polymeric membranes: a review, J. Mater. Chem. A 5 (2017) 6776–6793, http://dx.doi.org/10.1039/C7TA00009J.
[34] H. Ji, H. Sun, X. Qu, Antibacterial applications of graphene-based nanomaterials: recent achievements and challenges, Adv. Drug Deliv. Rev. 105 (2016) 176–189, http://dx.doi.org/10.1016/j.addr.2016.04.009.
[35] A. Wanag, P. Rokicka, E. Kusiak-Nejman, J. Kapica-Kozar, R.J. Wrobel, A. Markowska-Szczupak, A.W. Morawski, Antibacterial properties of TiO_2 modified with reduced graphene oxide, Ecotoxicol. Environ. Saf. 147 (2018) 788–793, http://dx.doi.org/10.1016/j.ecoenv.2017.09.039.
[36] Y.-N. Chang, X.-M. Ou, G.-M. Zeng, J.-L. Gong, C.-H. Deng, Y. Jiang, J. Liang, G.-Q. Yuan, H.-Y. Liu, X. He, Synthesis of magnetic graphene oxide–TiO_2 and their antibacterial properties under solar irradiation, Appl. Surf. Sci. 343 (2015) 1–10, http://dx.doi.org/10.1016/j.apsusc.2015.03.082.
[37] R. Rahimi, S. Zargari, A. Yousefi, M. Yaghoubi Berijani, A. Ghaffarinejad, A. Morsali, Visible light photocatalytic disinfection of *E. coli* with TiO_2–graphene nanocomposite sensitized with tetrakis(4-carboxyphenyl)porphyrin, Appl. Surf. Sci. 355 (2015) 1098–1106, http://dx.doi.org/10.1016/j.apsusc.2015.07.115.
[38] L. Karimi, M.E. Yazdanshenas, R. Khajavi, A. Rashidi, M. Mirjalili, Using graphene/TiO_2 nanocomposite as a new route for preparation of electroconductive, self-cleaning, antibacterial and antifungal cotton fabric without toxicity, Cellulose 21 (2014) 3813–3827, http://dx.doi.org/10.1007/s10570-014-0385-1.
[39] P. Gao, A. Li, D.D. Sun, W.J. Ng, Effects of various TiO_2 nanostructures and graphene oxide on photocatalytic activity of TiO_2, J. Hazard. Mater. 279 (2014) 96–104, http://dx.doi.org/10.1016/j.jhazmat.2014.06.061.
[40] L. Liu, H. Bai, J. Liu, D.D. Sun, Multifunctional graphene oxide-TiO_2-Ag nanocomposites for high performance water disinfection and decontamination under solar irradiation, J. Hazard. Mater. 261 (2013) 214–223, http://dx.doi.org/10.1016/j.jhazmat.2013.07.034.
[41] B. Cao, S. Cao, P. Dong, J. Gao, J. Wang, High antibacterial activity of ultrafine TiO_2/graphene sheets nanocomposites under visible light irradiation, Mater. Lett. 93 (2013) 349–352, http://dx.doi.org/10.1016/j.matlet.2012.11.136.
[42] J. Liu, L. Liu, H. Bai, Y. Wang, D.D. Sun, Gram-scale production of graphene oxide–TiO_2 nanorod composites: towards high-activity photocatalytic materials, Appl. Catal. B Environ. 106 (2011) 76–82, http://dx.doi.org/10.1016/j.apcatb.2011.05.007.
[43] O. Akhavan, E. Ghaderi, Photocatalytic Reduction of Graphene Oxide Nanosheets on TiO_2 Thin Film for Photoinactivation of Bacteria in Solar Light Irradiation, (2009) http://pubs.acs.org/doi/abs/10.1021/jp906325q . (Accessed 24 January 2016).
[44] Official Journal of the European Union: Commission Implementing Decision (EU) 2015/495 of 20 March 2015 establishing a watch list of substances for Union-wide monitoring in the field of water policy pursuant to Directive 2008/105/EC of the European Parliament and of the council (2015). Available at: http://data.europa.eu/eli/dec_impl/2015/495/oj.
[45] W.S. Hummers, R.E. Offeman, Preparation of Graphitic Oxide, J. Am. Chem. Soc. 80 (1958) 1339, http://dx.doi.org/10.1021/ja01539a017.
[46] W. Fan, Q. Lai, Q. Zhang, Y. Wang, Nanocomposites of TiO_2 and reduced graphene oxide as efficient photocatalysts for hydrogen evolution, J. Phys. Chem. C 115 (2011) 10694–10701, http://dx.doi.org/10.1021/jp2008804.
[47] G. Williams, B. Seger, P.V. Kamat, TiO_2-graphene nanocomposites. UV-assisted photocatalytic reduction of graphene oxide, ACS Nano 2 (2008) 1487–1491, http://dx.doi.org/10.1021/nn800251f.
[48] E.S. Galbavy, K. Ram, C. Anastasio, 2-Nitrobenzaldehyde as a chemical actinometer for solution and ice photochemistry, J. Photochem. Photobiol. A Chem. 209 (2010) 186–192, http://dx.doi.org/10.1016/j.jphotochem.2009.11.013.
[49] M. Gros, M. Petrović, D. Barceló, Wastewater treatment plants as a pathway for aquatic contamination by pharmaceuticals in the Ebro river basin (Northeast Spain), Environ. Toxicol. Chem. 26 (2007) 1553, http://dx.doi.org/10.1897/06-495R.1.
[50] Clinical and Laboratory Standards Institute, Performance standards for antimicrobial susceptibility testing; twenty second informational supplement, M100-S22, CLSI, Wayne, PA, 2012http://clsi.org//.
[51] J. Oliver, The viable but nonculturable state in bacteria, J. Microbiol. 43 (2005) 93–100 https://www.researchgate.net/profile/James_Oliver4/publication/7969638_The_Viable_but_Nonculturable_State_in_Bacteria/links/00b7d51e5521d33219000000/The-Viable-but-Nonculturable-State-in-Bacteria.pdf . (Accessed 18 July 2017).
[52] D.A. Ratkowsky, J. Olley, T.A. McMeekin, A. Ball, Relationship between temperature and growth rate of bacterial cultures, J. Bacteriol. 149 (1982) 1–5 http://jb.asm.org/content/149/1/1.abstract.
[53] M.F. Davis, S.A. Iverson, P. Baron, A. Vasse, E.K. Silbergeld, E. Lautenbach, D.O. Morris, Household transmission of meticillin-resistant *Staphylococcus aureus* and other staphylococci, Lancet Infect. Dis. 12 (2012) 703–716, http://dx.doi.org/10.1016/S1473-3099(12)70156-1.
[54] J. Alexander, A. Bollmann, W. Seitz, T. Schwartz, Microbiological characterization of aquatic microbiomes targeting taxonomical marker genes and antibiotic resistance genes of opportunistic bacteria, Sci. Total Environ. 512–513 (2015) 316–325, http://dx.doi.org/10.1016/j.scitotenv.2015.01.046.
[55] M. Gros, M. Petrović, D. Barceló, Development of a multi-residue analytical methodology based on liquid chromatography–tandem mass spectrometry (LC–MS/MS) for screening and trace level determination of pharmaceuticals in surface and wastewaters, Talanta 70 (2006) 678–690, http://dx.doi.org/10.1016/j.talanta.2006.05.024.
[56] D.M. Tobaldi, R.C. Pullar, A.S. Škapin, M.P. Seabra, J.A. Labrincha, Visible light activated photocatalytic behaviour of rare earth modified commercial TiO_2, Mater. Res. Bull. 50 (2014) 183–190, http://dx.doi.org/10.1016/j.materresbull.2013.10.033.
[57] S. Reich, C. Thomsen, Raman spectroscopy of graphite, Philos. Trans. R. Soc. Lond. A Math. Phys. Eng. Sci. 362 (2004).
[58] K.N. Kudin, B. Ozbas, H.C. Schniepp, R.K. Prud'homme, I.A. Aksay, R. Car, Raman spectra of graphite oxide and functionalized graphene sheets, Nano Lett. 8 (2007) 36–41, http://dx.doi.org/10.1021/NL071822Y.
[59] S. Wang, H. Sun, H.M. Ang, M.O. Tadé, Adsorptive remediation of environmental pollutants using novel graphene-based nanomaterials, Chem. Eng. J. 226 (2013) 336–347, http://dx.doi.org/10.1016/j.cej.2013.04.070.
[60] L. Hu, P.M. Flanders, P.L. Miller, T.J. Strathmann, Oxidation of sulfamethoxazole and related antimicrobial agents by TiO2 photocatalysis, Water Res. 41 (2007) 2612–2626, http://dx.doi.org/10.1016/j.watres.2007.02.026.
[61] N.P. Xekoukoulotakis, C. Drosou, C. Brebou, E. Chatzisymeon, E. Hapeshi, D. Fatta-Kassinos, D. Mantzavinos, Kinetics of UV-A/TiO_2 photocatalytic degradation and mineralization of the antibiotic sulfamethoxazole in aqueous matrices, Catal. Today 161 (2011) 163–168, http://dx.doi.org/10.1016/j.cattod.2010.09.027.
[62] M.N. Abellán, B. Bayarri, J. Giménez, J. Costa, Photocatalytic degradation of sulfamethoxazole in aqueous suspension of TiO_2, Appl. Catal. B Environ. 74 (2007) 233–241, http://dx.doi.org/10.1016/j.apcatb.2007.02.017.
[63] N.P. Xekoukoulotakis, N. Xinidis, M. Chroni, D. Venieri, E. Hapeshi, D. Fatta-Kassinos, D. Mantzavinos, D. Venieri, E. Hapeshi, D. Fatta-Kassinos, UV-A/TiO_2 photocatalytic decomposition of erythromycin in water: factors affecting mineralization and antibiotic activity, Catal. Today 151 (2010) 29–33, http://dx.doi.org/10.1016/j.cattod.2010.01.040.
[64] K. Vignesh, M. Rajarajan, A. Suganthi, Photocatalytic degradation of erythromycin under visible light by zinc phthalocyanine-modified titania nanoparticles, Mater. Sci. Semicond. Process. 23 (2014) 98–103, http://dx.doi.org/10.1016/j.mssp.2014.02.050.
[65] M.N. Mordi, M.D. Pelta, V. Boote, G.A. Morris, J. Barber, Acid-catalyzed degradation of clarithromycin and erythromycin B: a comparative study using NMR spectroscopy, J. Med. Chem. 43 (2000) 467–474, http://dx.doi.org/10.1021/

jm9904811.
[66] C. Abegglen, A. Joss, C.S. McArdell, G. Fink, M.P. Schlüsener, T.A. Ternes, H. Siegrist, The fate of selected micropollutants in a single-house MBR, Water Res. 43 (2009) 2036–2046, http://dx.doi.org/10.1016/j.watres.2009.02.005.
[67] A. Göbel, A. Thomsen, C.S. McArdell, A.C. Alder, W. Giger, N. Theiß, D. Löffler, T.A. Ternes, Extraction and determination of sulfonamides, macrolides, and trimethoprim in sewage sludge, J. Chromatogr. A 1085 (2005) 179–189, http://dx.doi.org/10.1016/j.chroma.2005.05.051.
[68] C.S. McArdell, E. Molnar, M.J.-F. Suter, W. Giger, Occurrence and fate of macrolide antibiotics in wastewater treatment plants and in the Glatt Valley Watershed, Switzerland, Environ. Sci. Technol. 37 (2003) 5479–5486, http://dx.doi.org/10.1021/es034368i.
[69] P.S.M. Dunlop, C.P. Sheeran, J.A. Byrne, M.A.S. McMahon, M.A. Boyle, K.G. McGuigan, Inactivation of clinically relevant pathogens by photocatalytic coatings, J. Photochem. Photobiol. A Chem. 216 (2010) 303–310, http://dx.doi.org/10.1016/j.jphotochem.2010.07.004.
[70] E.R. Bandala, E. Bustos, A. Hernández-Ramírez, I. Medina-Ramírez (Eds.), Photocatalytic Semiconductors, Springer International Publishing, Cham, 2015, pp. 255–278, , http://dx.doi.org/10.1007/978-3-319-10999-2.
[71] J. Süß, S. Volz, U. Obst, T. Schwartz, Application of a molecular biology concept for the detection of DNA damage and repair during UV disinfection, Water Res. 43 (2009) 3705–3716, http://dx.doi.org/10.1016/j.watres.2009.05.048.
[72] H.A. Foster, I.B. Ditta, S. Varghese, A. Steele, Photocatalytic disinfection using titanium dioxide: spectrum and mechanism of antimicrobial activity, Appl. Microbiol. Biotechnol. 90 (2011) 1847–1868, http://dx.doi.org/10.1007/s00253-011-3213-7.
[73] P.-C. Maness, S. Smolinski, D.M. Blake, Z. Huang, E.J. Wolfrum, W.A. Jacoby, Bactericidal activity of photocatalytic TiO_2 reaction: toward an understanding of its killing mechanism, Appl. Environ. Microbiol. 65 (1999) 4094–4098 http://aem.asm.org/content/65/9/4094.short . (Accessed 24 January 2016).
[74] Z. Huang, P.-C. Maness, D.M. Blake, E.J. Wolfrum, S.L. Smolinski, W.A. Jacoby, Bactericidal mode of titanium dioxide photocatalysis, J. Photochem. Photobiol. A Chem. 130 (2000) 163–170, http://dx.doi.org/10.1016/S1010-6030(99)00205-1.
[75] K. Sunada, T. Watanabe, K. Hashimoto, Studies on photokilling of bacteria on TiO_2 thin film, J. Photochem. Photobiol. A Chem. 156 (2003) 227–233, http://dx.doi.org/10.1016/S1010-6030(02)00434-3.
[76] X.-C. Shen, Z.-L. Zhang, B. Zhou, J. Peng, M. Xie, M. Zhang, D.-W. Pang, Visible light-induced plasmid DNA damage catalyzed by a XdSe/ZnS-photosensitized nano-TiO_2 film, Environ. Sci. Technol. 42 (2008) 5049–5054, http://dx.doi.org/10.1021/es800668g.
[77] T.-M. Tsai, H.-H. Chang, K.-C. Chang, Y.-L. Liu, C.-C. Tseng, A comparative study of the bactericidal effect of photocatalytic oxidation by TiO_2 on antibiotic-resistant and antibiotic-sensitive bacteria, J. Chem. Technol. Biotechnol. 85 (2010) 1642–1653, http://dx.doi.org/10.1002/jctb.2476.
[78] T. Sato, M. Taya, Enhancement of phage inactivation using photocatalytic titanium dioxide particles with different crystalline structures, Biochem. Eng. J. 28 (2006) 303–308, http://dx.doi.org/10.1016/j.bej.2006.01.004.
[79] L. Liu, J. Liu, D.D. Sun, Graphene oxide enwrapped Ag_3PO_4 composite: towards a highly efficient and stable visible-light-induced photocatalyst for water purification, Catal. Sci. Technol. 2 (2012) 2525, http://dx.doi.org/10.1039/c2cy20483e.
[80] G. Gogniat, S. Dukan, TiO_2 photocatalysis causes DNA damage via fenton reaction-generated hydroxyl radicals during the recovery period, Appl. Environ. Microbiol. 73 (2007) 7740–7743, http://dx.doi.org/10.1128/AEM.01079-07.
[81] K. Hirakawa, M. Mori, M. Yoshida, S. Oikawa, S. Kawanishi, Photo-irradiated titanium dioxide catalyzes site specific DNA damage via generation of hydrogen peroxide, Free Radic. Res. (2009) http://www.tandfonline.com/doi/abs/10.1080/10715760420002064870 . (Accessed 24 January 2016).
[82] S. Pigeot-Rémy, F. Simonet, E. Errazuriz-Cerda, J.C. Lazzaroni, D. Atlan, C. Guillard, Photocatalysis and disinfection of water: identification of potential bacterial targets, Appl. Catal. B Environ. 104 (2011) 390–398, http://dx.doi.org/10.1016/j.apcatb.2011.03.001.
[83] S. Giannakis, E. Darakas, A. Escalas-Cañellas, C. Pulgarin, Elucidating bacterial regrowth: effect of disinfection conditions in dark storage of solar treated secondary effluent, J. Photochem. Photobiol. A Chem. 290 (2014) 43–53, http://dx.doi.org/10.1016/j.jphotochem.2014.05.016.
[84] H. Volkmann, T. Schwartz, P. Bischoff, S. Kirchen, U. Obst, Detection of clinically relevant antibiotic-resistance genes in municipal wastewater using real-time PCR (TaqMan), J. Microbiol. Methods 56 (2) (2004) 277–286, http://dx.doi.org/10.1016/j.mimet.2003.10.014.
[85] N. Czekalski, T. Berthold, S. Caucci, A. Egli, H. Bürgmann, Increased levels of multiresistant bacteria and resistance genes after wastewater treatment and their dissemination into lake geneva, Switzerland, Front. Microbiol. 3 (2012) 106, http://dx.doi.org/10.3389/fmicb.2012.00106.
[86] R.J. Clifford, M. Milillo, J. Prestwood, R. Quintero, D.V. Zurawski, Y.I. Kwak, P. Mc Gann, Detection of bacterial 16S rRNA and identification of four clinically important bacteria by real-time PCR, PLoS One 7 (11) (2012) e48558, http://dx.doi.org/10.1371/journal.pone.0048558.